Decoherence of a driven multilevel quantum system interacting with a multi-bath reservoir

Zhongyuan Zhou[1,2], Shih-I Chu[1], and Siyuan Han[2]

[1]*Department of Chemistry, University of Kansas, Lawrence, KS 66045*

[2]*Department of Physics and Astronomy,*

University of Kansas, Lawrence, KS 66045

(Received: February 1, 2008)

Abstract

A general theory is presented for the treatment of decoherence of a multilevel quantum system (with many degrees of freedom) interacting with multi-bath reservoir and driven by ac fields. In this approach, the system is described by a reduced density operator and the multi-bath reservoir is characterized by a number of spectral densities. The reduced density operator is governed by the master equation in which the effect of ac driving fields and the leakage to non-computational states are included. The theory is applied to the study of decoherence of a two-dimensional (2D) SQUID flux qubit coupled to control and readout circuits. The predicted results are in very good agreement with available experimental results in the absence of driving fields and with the analytic results of a dissipative two-level system in the presence of weak driving fields. The relaxation and decoherence times versus the parameters and temperature of the control and readout circuits are also explored in details to facilitate the optimization of the 2D SQUID qubit.

PACS numbers: 85.25.-j, 03.67.Lx, 76.60.Es

I. INTRODUCTION

In the past few years, solid-state qubits based on superconducting devices are of particular interest for quantum computation because of their advantages of large-scale integration, flexibility in design, and easy connection to conventional electronic circuits[1]. Significant progress has been made on physical implementation of quantum computation based on superconducting qubits. Quantum coherence has been successfully demonstrated in a variety of superconducting single-qubit systems[2,3,4,5,6,7,8,9] and coupled two-qubit systems.[10,11,12,13] However, all the superconducting qubits demonstrated in the experiments so far have relatively short coherence time and high probability of gate errors.[2,3,4,5,8,9,10,11] One of the causes of these problems is the intrinsic gate error resulting from leakage to non-computational states due to the typical multilevel structures of superconducting qubits.[14,15] This kind of gate error has been explored[14,15,16] and can be minimized by using appropriate working parameters for the qubits with their device parameters given *in prior*.[16] Another cause is the extrinsic gate error arising from coupling between the qubits and environment resulting in decoherence such as relaxation and dephasing.[17,18] Due to the unavoidable coupling with environment, the superconducting qubits always suffer from such kind of extrinsic gate error. Thus the environment-induced decoherence is one of the main obstacles to the practical application of superconducting qubits in quantum computation.[1,3,17,19,20]

The typical environment in superconducting qubits is electronic circuits used for control and readout of the qubits. Although the decoherence of superconducting qubits induced by such kind of environment has been extensively investigated both theoretically[1,17,18,21,22,23,24,25,26,27,28,29,30,31,32,33,34,35] and experimentally.[3,9,19,26,29,36,37,38,39,40,41,42], almost all the investigations so far are for the qubits in the absence of driving fields (free decay). However, in superconducting-qubit based quantum computation, ac fields (e.g., microwave fields) are usually used to manipulate the qubit's states.[2,3,4,5,6,7,8,9,10,11,12,13,23] Due to the coupling of the qubits with the fields the effect of driving fields and leakage to non-computational states may be quite large depending on the field strength[14,15,16] and thus the dynamics of driven qubits may be quite different from that of qubits in free decay. Recent experiment[20] shows that the decoherence time of a superconducting qubit is significantly increased in the presence of a resonantly ac driving field. Thus a through investigation of decoherence of realistic superconducting qubits needs to include effect of driving fields and leakage to non-computational states.[23]

Furthermore, building a practical quantum computer requires simultaneous operations of a large number of multiqubit gates in a coupled multiqubit system.[43,44,45] On one hand, the coupled

multiqubit system may have many degrees of freedom, on the other hands, due to complexity and diversity of the superconducting circuits, the environment may be a multibath one. In this case, the coupled multiqubit system may interact with the environment through all the degrees of freedom *simultaneously*, resulting in significantly different decoherence from that interacting with the environment through one degree of freedom of single qubits. Therefore, to investigate the decoherence of coupled superconducting qubits in realistic gate operations of quantum computation, one needs an approach for a quantum system of many degrees of freedom interacting with a multibath reservoir and driven by ac fields.

In this paper, we propose a general theory for the treatment of decoheerence of a multilevel quantum system of many degrees of freedom interacting with a multibath reservoir and driven by ac fields. In this theory, the multibath reservoir are characterized by a number of spectral densities.[46,47,48] For superconducting qubits coupled to electronic circuits, the spectral densities at finite temperature can be calculated in terms of recently proposed approaches[21,48] together with the quantum fluctuation-dissipation theorem.[47,48] The system is described by a reduced density operator. The reduced density operator is governed by the master equation in which the effect of driving fields and leakage due to the driving field and reservoir are included. This theory is used to simulate the dynamic process of a two-dimensional (2D) superconducting quantum interface device (SQUID) flux qubit coupled to control and readout circuits in the absence of driving fields (free decay). The results are in very good agreement with the available experimental results. It is also applied to investigate the effect of driving fields on the decoherence of the 2D SQUID qubit coupled to the control and readout circuits and driven by a resonant microwave field. The results agree well with the analytical results of the dissipative two-level system in the case of weak driving fields. To optimize the 2D SQUID qubit, the changes of relaxation and decoherence times versus the parameters and temperature of the control and readout circuits are explored.

II. MASTER EQUATION OF A DRIVEN OPEN QUANTUM SYSTEM

A. General form of master equation for a driven open quantum system

In general, an open quantum system is described by a generalized master equation of non-Markovian process.[27,49,50,51] However, in the case of weak damping and weak driving fields, which is the case for most of superconducting (charge, flux, and phase) qubits, the generalized non-Markovian master equation is equivalent to the Markovian master equation.[49,51] Thus we will

present the dissipative theory for Markovian process.

Let us consider a global system consisting of a quantum system surrounded by a reservoir and driven by an ac field. If the interaction of the driving field and reservoir is neglected, the Hamiltonian of the global system can be written as

$$H_G = H_S + H_R + H_I + H_F, \tag{1}$$

where, H_S is the Hamiltonian of the quantum system, H_R is the Hamiltonian of the reservoir, H_I is the interaction of the quantum system and reservoir, and H_F is the interaction of the quantum system and driving field. Obviously H_R commutes with both H_S and H_F. For the case of weak damping and weak driving field considered here, the interactions H_I and H_F are proportional to the system's coordinate operators linearly and thus they also commute with each other.[52]

In Schrödinger picture, the motion of the global system is described by *Liouville-von Neumann* equation[53]

$$\frac{d\eta(t)}{dt} = -\frac{i}{\hbar}\left[H_G(t), \eta(t)\right] = -i\mathcal{L}(t)\eta(t), \tag{2}$$

where, $\eta(t)$ is the density operator of the global system and $\mathcal{L}(t)$ is the Liouville superoperator corresponding to the Hamiltonian of the global system defined by

$$\mathcal{L} = \frac{1}{\hbar}\left[H_G, \right] = \mathcal{L}_S + \mathcal{L}_R + \mathcal{L}_I + \mathcal{L}_F. \tag{3}$$

Here, $\mathcal{L}_q = \left[H_q, \right]/\hbar$ is the Liouville superoperator corresponding to the Hamiltonian H_q for $q = S$, R, I, and F. The density operator of the global system satisfies $\mathrm{Tr}_{S,R}\eta(t) = 1$, where $\mathrm{Tr}_{S,R}$ is the trace over both the quantum system and reservoir.

In the global system, the quantum system performs a dissipative process due to the coupling with reservoir. This process can be characterized by a reduced density operator $\rho(t)$. It is calculated by tracing $\eta(t)$ over the reservoir

$$\rho(t) = \mathrm{Tr}_R\eta(t). \tag{4}$$

In the case of weak field and weak damping, $\rho(t)$ is governed by the master equation which, in Schrödinger picture, is given by (see Appendix A for details)

$$\frac{d\rho(t)}{dt} = -i\left[\mathcal{L}_S + \mathcal{L}_F(t)\right]\rho(t) + \mathcal{D}_I(t)\rho(t), \tag{5}$$

where, $\mathcal{D}_I(t)$ is the dissipation superoperator given by Eq. (A13). On the right-hand side of Eq. (5), the first term describes the coherent dynamics of the unperturbed quantum system, the second

term represents the pumping dynamics of the driving field, and the third term which is called the dissipator[53] characterizes the dissipative dynamics due to the interaction of the quantum system and reservoir. The dissipator includes all the information of dissipative dynamics.[54] Note that Eq. (5) is determined only by the operators at present and no longer depends on the operators in the past. Thus it describes a Markovian process of the quantum system[52]. The Markovian process is irreversible because the energy transferred to the reservoir can no longer return to the quantum system completely. In the case of weak damping and weak driving fields the Markovian approximation is equivalent to the non-Markovian approach.[49,51]

B. Master equation of a driven quantum system of many degrees of freedom interacting with a multibath reservoir

Let us consider a quantum system of many degrees of freedom encompassed by a multibath reservoir and driven by an ac field. The multibath can be separated into a number of independent baths. They have different properties and interact with the system via different degrees of freedom. If interactions between the baths are incorporated into the Hamiltonian of the reservoir, the total interaction H_I of the system and the multibath reservoir is given by[52,55]

$$H_I(t) = \sum_{\mu} X_{\mu}(t)\varsigma_{\mu}(t), \tag{6}$$

where, $\varsigma_{\mu}(t)$ is the operator of the μth bath of the reservoir, $X_{\mu}(t)$ is the system operator corresponding to the μth bath, and the sum to μ is over all the baths of the reservoir and all the degrees of freedom of the system. In general, the interaction $H_I(t)$ is a Hermitian operator but X_{μ} and ς_{μ} may be non-Hermitian. In the case of weak damping, $X_{\mu}(t)$ is reduced to the system coordinate operator and $\varsigma_{\mu}(t)$ is reduced to the fluctuation force of the μth bath.[46,47] For a driven quantum system of many degrees of freedom interacting with a multibath reservoir, the reduced density operator of the system still satisfies the maser equation given by Eq. (5). Using Eqs. (3), (6), (A5), (A13), and (A14), the dissipator $\mathcal{D}_I(t)\rho(t)$ in Eq. (5) is now given by

$$\begin{aligned}\mathcal{D}_I(t)\rho(t) \;=\; & \frac{1}{\hbar^2}\sum_{\mu,\nu}\int_0^t \Big[X_{\mu}(t)\,\rho(t)\,\widetilde{X}_{\nu}(\tau)\,\mathcal{J}_{\mu\nu}(\tau) \\ & -X_{\mu}(t)\,\widetilde{X}_{\nu}(\tau)\,\rho(t)\,\mathcal{J}^{\dagger}_{\nu\mu}(-\tau) \\ & -\rho(t)\,\widetilde{X}_{\nu}(\tau)\,X_{\mu}(t)\,\mathcal{J}_{\mu\nu}(\tau) \\ & +\widetilde{X}_{\nu}(\tau)\,\rho(t)\,X_{\mu}(t)\,\mathcal{J}^{\dagger}_{\nu\mu}(-\tau)\Big]\,d\tau,\end{aligned} \tag{7}$$

where, $\widetilde{X}_\mu$ is the representation of X_μ in the interaction picture given by

$$\widetilde{X}_\mu(-\tau) = \exp\left(\frac{i}{\hbar}H_S\tau\right) X_\mu(t+\tau) \exp\left(-\frac{i}{\hbar}H_S\tau\right), \tag{8}$$

and $\mathcal{J}_{\mu\nu}(\tau)$ and $\mathcal{J}^\dagger_{\nu\mu}(-\tau)$ are the two kinds of correlation functions of the fluctuation forces between the μth and νth baths. The correlation function $\mathcal{J}_{\mu\nu}(\tau)$ is defined by

$$\begin{aligned} \mathcal{J}_{\mu\nu}(\tau) &= \mathrm{Tr}_R\left[\widetilde{\varsigma}_\mu(t)\sigma(R)\widetilde{\varsigma}_\nu(t-\tau)\right] \\ &= \langle\widetilde{\varsigma}_\mu(t)\widetilde{\varsigma}_\nu(t-\tau)\rangle, \end{aligned} \tag{9}$$

where, $\widetilde{\varsigma}_\mu$ is the representation of ς_μ in the interaction picture defined by

$$\widetilde{\varsigma}_\mu(\tau) = \exp\left(\frac{i}{\hbar}H_R\tau\right) \varsigma_\mu(\tau) \exp\left(-\frac{i}{\hbar}H_R\tau\right). \tag{10}$$

The correlation function $\mathcal{J}^\dagger_{\nu\mu}(-\tau)$ is the complex transpose of $\mathcal{J}_{\mu\nu}(\tau)$. In general, since $\widetilde{\varsigma}_\mu(t)$ and $\widetilde{\varsigma}_\nu(t-\tau)$ may not be Hermitian operators and/or they do not commute with each other, $\mathcal{J}_{\mu\nu}(\tau)$ is a non-Hermitian matrix and $\mathcal{J}^\dagger_{\nu\mu}(-\tau) \neq \mathcal{J}_{\mu\nu}(\tau)$.

If the μth bath does not interact with the νth bath, the correlation between the two baths is zero. In this case, the correlation function $\mathcal{J}_{\mu\nu}(\tau)$ can be written as

$$\mathcal{J}_{\mu\nu}(\tau) = \mathcal{J}_{\mu\mu}(\tau)\,\delta_{\mu\nu}, \tag{11}$$

where, $\mathcal{J}_{\mu\mu}(\tau)$ is the autocorrelation function. The autocorrelation function $\mathcal{J}_{\mu\mu}(\tau)$ represents the correlation of the bath state at time $t-\tau$ to the bath state at time t, while the autocorrelation function $\mathcal{J}^\dagger_{\mu\mu}(-\tau)$ represents the correlation of the bath state at time t to the bath state at time $t-\tau$. In general, $\mathcal{J}^\dagger_{\mu\mu}(-\tau) \neq \mathcal{J}_{\mu\mu}(\tau)$, which signifies the irreversibility in time of the correlation function. From Eq. (9), the irreversibility is attributed to the non-Hermitian property and/or noncommutable property of the reservoir operators.

From Eq. (7), the effect of reservoir on the system is represented by the correlation function $\mathcal{J}(t)$. It is difficult to calculate the correlation function directly from the fluctuation forces of the reservoir. In reality, the effect of reservoir on the system can be equivalently characterized by a real and measurable spectral density of the reservoir[46,47,48]. The relation between the correlation function $\mathcal{J}(t)$ and the spectral density $J_\varsigma(\omega)$ is given by the Wiener-Khintchine theorem[56]

$$\mathcal{J}(t) = \frac{1}{2\pi}\int_{-\infty}^{+\infty} J_\varsigma(\omega)\exp(i\omega t)\,d\omega, \tag{12}$$

and

$$J_\varsigma(\omega) = \int_{-\infty}^{+\infty} \mathcal{J}(t)\exp(-i\omega t)\,dt. \tag{13}$$

For solid-state qubits, particularly for the superconducting qubits consisting of electronic circuits, the spectral density at zero temperature can be calculated in terms of the recently proposed approaches.[21,48] The spectral density at finite temperature can be obtained from the zero-temperature spectral density by means of the quantum fluctuation-dissipation theorem[47,48].

III. REPRESENTATION OF MASTER EQUATION IN HILBERT SPACE

A. Representation in an arbitrary Hilbert space

Suppose $\{|n\rangle\}$ is a complete basis set of the system. In the Hilbert space spanned by $\{|n\rangle\}$, the reduced density operator ρ is represented by a density matrix with matrix elements given by

$$\rho_{mn}(t) = \langle m|\rho(t)|n\rangle . \tag{14}$$

The diagonal matrix element ρ_{mm} and off-diagonal matrix element ρ_{mn} $(m \neq n)$ are the population of state $|m\rangle$ and coherence of states $|m\rangle$ and $|n\rangle$, respectively. From Eqs. (5) and (7), the density matrix element $\rho_{mn}(t)$ satisfies the master equation

$$\begin{aligned}\frac{d\rho_{mn}(t)}{dt} &= -i\sum_{m'n'}\left[\mathcal{L}^{S}_{mn,m'n'} + \mathcal{L}^{F}_{mn,m'n'}\right]\rho_{m'n'} \\ &\quad + \sum_{m'n'}\mathcal{D}^{I}_{mn,m'n'}\rho_{m'n'},\end{aligned} \tag{15}$$

where, $\mathcal{L}^{S}_{mn,m'n'}$ and $\mathcal{L}^{F}_{mn,m'n'}$ are the matrix elements of $\mathcal{L}_S$ and $\mathcal{L}_F$, respectively, and $\mathcal{D}^{I}_{mn,m'n'}$ is the dissipation matrix element of the dissipation superoperator $\mathcal{D}_I$ describing the effect of the reservoir on the system. They are given by

$$\mathcal{L}^{\Theta}_{mn,m'n'} = \frac{1}{\hbar}\left[H^{\Theta}_{mm'}\delta_{n'n} - H^{\Theta}_{n'n}\delta_{mm'}\right], \tag{16}$$

and

$$\begin{aligned}\mathcal{D}^{I}_{mn,m'n'} &= \frac{1}{\hbar^2}\sum_{\mu,\nu}\int_0^t \Big[X^{\mu}_{mm'}(t)\,\widetilde{X}^{\nu}_{n'n}(\tau)\,\mathcal{J}_{\mu\nu}(\tau) \\ &\quad -\delta_{nn'}\sum_k X^{\mu}_{mk}(t)\,\widetilde{X}^{\nu}_{km'}(\tau)\,\mathcal{J}^{\dagger}_{\nu\mu}(-\tau) \\ &\quad -\delta_{mm'}\sum_k \widetilde{X}^{\nu}_{n'k}(\tau)\,X^{\mu}_{kn}(t)\,\mathcal{J}_{\mu\nu}(\tau) \\ &\quad + \widetilde{X}^{\nu}_{mm'}(\tau)\,X^{\mu}_{n'n}(t)\,\mathcal{J}^{\dagger}_{\nu\mu}(-\tau)\Big]\,d\tau,\end{aligned} \tag{17}$$

where, $H^{\Theta}_{mn} = \langle m|H_{\Theta}|n\rangle$ for $\Theta = S$ and F, and $X^{\alpha}_{mn}(t) = \langle m|X_{\alpha}(t)|n\rangle$ and $\widetilde{X}^{\alpha}_{mn}(t) = \left\langle m\left|\widetilde{X}_{\alpha}(t)\right|n\right\rangle$ for $\alpha = \mu$ and ν.

B. Representation in the Hilbert space of Hamiltonian eigenstates

Suppose E_n and $|n\rangle$ are respectively the eigenvalue and eigenfunction of H_S obtained by solving the eigenvalue equation $H_S|n\rangle = E_n|n\rangle$. In the Hilbert space spanned by the eigenstates $\{|n\rangle\}$, the density matrix element and the master equation are still given by Eq. (14) and Eq. (15), respectively. But now the matrix elements $\mathcal{L}^S_{mn,m'n'}$ and $\mathcal{L}^F_{mn,m'n'}$ are simplified to

$$\mathcal{L}^S_{mn,m'n'} = \omega_{mn}\delta_{mm'}\delta_{nn'}, \tag{18}$$

and

$$\mathcal{L}^F_{mn,m'n'} = \frac{1}{\hbar}\left[H^F_{mm'}(t)\delta_{nn'} - H^F_{n'n}(t)\delta_{mm'}\right], \tag{19}$$

where, $\omega_{mn} = (E_m - E_n)/\hbar$ and $H^F_{mn}(t) = \langle m|H_F(t)|n\rangle$. The matrix element $\mathcal{D}^I_{mn,m'n'}$ in Eq. (17) is also simplified to

$$\begin{aligned}\mathcal{D}^I_{mn,m'n'} \;=\; & \frac{1}{\hbar^2}\sum_{\mu,\nu}\int_0^t \Big[X^\mu_{mm'}(t)\,X^\nu_{n'n}\left(t'\right)e^{i\omega_{nn'}\tau}\mathcal{J}_{\mu\nu}(\tau) \\ & -\delta_{nn'}\sum_k X^\mu_{mk}(t)\,X^\nu_{km'}\left(t'\right)e^{i\omega_{m'k}\tau}\mathcal{J}^\dagger_{\nu\mu}(-\tau) \\ & -\delta_{mm'}\sum_k X^\nu_{n'k}\left(t'\right)X^\mu_{kn}(t)\,e^{i\omega_{kn'}\tau}\mathcal{J}_{\mu\nu}(\tau) \\ & + X^\nu_{mm'}\left(t'\right)X^\mu_{n'n}(t)\,e^{i\omega_{m'm}\tau}\mathcal{J}^\dagger_{\nu\mu}(-\tau)\Big]\,d\tau,\end{aligned} \tag{20}$$

where, $t' = t - \tau$.

If the Hamiltonian eigenfunctions $\{|n\rangle\}$ are real, one has $H^F_{mn} = H^F_{nm}$ for the Hermitian operator $H_F(t)$. From Eqs. (18) and (19), the matrix elements $\mathcal{L}^\Theta_{mn,m'n'}$ for $\Theta = S$ and F have the following symmetric relations

$$\mathcal{L}^\Theta_{nm,n'm'} = -\mathcal{L}^\Theta_{mn,m'n'}, \tag{21}$$

and

$$\mathcal{L}^\Theta_{m'n',mn} = \mathcal{L}^\Theta_{mn,m'n'}. \tag{22}$$

From Eq. (21) one has $\mathcal{L}^\Theta_{mm,nn} = 0$.

If X_μ is time-independent, the matrix elements $\mathcal{D}^I_{mn,m'n'}$ can be further simplified. Introduce a function $F_{\mu\nu}(\omega,t)$ by

$$F_{\mu\nu}(\omega,t) = \int_0^t e^{i\omega\tau}\mathcal{J}_{\mu\nu}(\tau)\,d\tau. \tag{23}$$

Applying Eq. (23) to Eq. (20) one obtains

$$\begin{aligned}\mathcal{D}^{I}_{mn,m'n'} &= \frac{1}{\hbar^2}\sum_{\mu,\nu}\big[X^{\mu}_{mm'}X^{\nu}_{n'n}F_{\mu\nu}(\omega_{nn'},t)\\ &\quad -\delta_{nn'}\sum_{k}X^{\mu}_{mk}X^{\nu}_{km'}F^{\dagger}_{\mu\nu}(\omega_{km'},t)\\ &\quad -\delta_{mm'}\sum_{k}X^{\nu}_{n'k}X^{\mu}_{kn}F_{\mu\nu}(\omega_{kn'},t)\\ &\quad + X^{\nu}_{mm'}X^{\mu}_{n'n}F^{\dagger}_{\mu\nu}(\omega_{mm'},t)\big], \end{aligned} \tag{24}$$

where $F^{\dagger}_{\mu\nu}(\omega,t)$ is the conjugate transpose of $F_{\mu\nu}(\omega,t)$. If the interaction between any two baths is negligible, $\mathcal{D}^{I}_{mn,m'n'}$ can be further simplified by using Eqs. (11) and (23). In this case, the correlation terms between different baths in Eq. (24) vanishes and thus the dissipation matrix element of the multibath reservoir is a sum of individual dissipation matrix element of each bath of the reservoir.

IF time-dependent part of X_μ is separable from system operators, X_μ can be expressed in a general form of Fourier series as

$$X_{\mu}(t)=\sum_{\lambda}\chi^{\mu}_{\lambda}\exp\left(i\omega^{\mu}_{\lambda}t\right), \tag{25}$$

where, χ^{μ}_{λ} is a time-independent operator that only depends on system operators.

Substituting Eq. (25) into Eq. (20) and using Eq. (23), one has

$$\begin{aligned}\mathcal{D}^{I}_{mn,m'n'} &= \frac{1}{\hbar^2}\sum_{\mu,\nu}\sum_{\lambda_1\lambda_2}\exp\left[i\left(\omega^{\mu}_{\lambda_1}+\omega^{\nu}_{\lambda_2}\right)t\right]\\ &\quad\times\Big[\chi^{\mu}_{\lambda_1,mm'}\chi^{\nu}_{\lambda_2,n'n}F_{\mu\nu}\left(\omega^{\nu-}_{\lambda_2,nn'},t\right)\\ &\quad -\delta_{nn'}\sum_{k}\chi^{\mu}_{\lambda_1,mk}\chi^{\nu}_{\lambda_2,km'}F^{\dagger}_{\mu\nu}\left(\omega^{\nu+}_{\lambda_2,km'},t\right)\\ &\quad -\delta_{mm'}\sum_{k}\chi^{\nu}_{\lambda_2,n'k}\chi^{\mu}_{\lambda_1,kn}F_{\mu\nu}\left(\omega^{\nu-}_{\lambda_2,kn'},t\right)\\ &\quad +\chi^{\nu}_{\lambda_2,mm'}\chi^{\mu}_{\lambda_1,n'n}F^{\dagger}_{\mu\nu}\left(\omega^{\nu+}_{\lambda_2,mm'},t\right)\Big], \end{aligned} \tag{26}$$

where, $\omega^{\nu\pm}_{\lambda_2,nn'}=\omega_{nn'}\pm\omega^{\nu}_{\lambda_2}$ and $\chi^{\alpha}_{\lambda,mn}=\langle m\left|\chi^{\alpha}_{\lambda}\right|n\rangle$ is the matrix element of the operator χ^{α}_{λ}.

Furthermore, if χ^{α}_{λ} is a time-independent operator that does not depend on system operators we have $\chi^{\alpha}_{\lambda,mn}=\langle m\left|\chi^{\alpha}_{\lambda}\right|n\rangle=\chi^{\alpha}_{\lambda}\delta_{mn}$. In this case, from Eq. (26) one has $\mathcal{D}^{I}_{mn,m'n'}=0$. Thus if the interaction of the system and reservoir does not depend on system operators, the reservoir does not have any effect on the system and thus they are decoupled.

IV. DISSIPATION OF A DRIVEN QUANTUM SYSTEM DUE TO A THERMAL BATH

One of the most popular and important reservoirs is a thermal bath. Due to the interaction with the thermal bath, the quantum system transits from one thermodynamic equilibrium state to another equilibrium state.[25] During this process, the spontaneous decay and stimulated transition follow the detailed balance principle. As has been demonstrated, if the interactions between the independent baths are neglected the dissipation matrix element of the multibath reservoir is a sum of individual dissipation matrix element of each bath. Thus in this section we will present the dissipative theory for a driven quantum system interacting with a thermal bath.

A. Lamb shift matrix and damping rate matrix

Suppose the driven quantum system is surrounded only by a sufficiently large thermal bath and the system operator X such as the system's canonical coordinate does not depend on time explicitly. From Eq. (24) the dissipation matrix element due to the thermal bath is now given by

$$\begin{aligned}\mathcal{D}^{I}_{mn,m'n'} &= \frac{1}{\hbar^2}\Bigg\{-\delta_{nn'}\sum_k X_{mk}X_{km'}F^*(\omega_{km'},t)\\ &\quad +X_{mm'}X_{n'n}\left[F(\omega_{nn'},t)+F^*(\omega_{mm'},t)\right]\\ &\quad -\delta_{mm'}\sum_k X_{n'k}X_{kn}F(\omega_{kn'},t)\Bigg\},\end{aligned} \tag{27}$$

where, the superscripts μ and ν are omitted for simplicity, $F(\omega,t)$ is given by Eq. (23), and $F^*(\omega,t)$ is the complex conjugate of $F(\omega,t)$.

If the spectral density of the thermal bath at temperature T is denoted by $J_\varsigma(\omega)$, the autocorrelation function $\mathcal{J}(t)$ can be calculated from $J_\varsigma(\omega)$ by Eq. (12). Substituting Eq. (12) into Eq. (23) we obtain

$$F(\omega,t)=F_R(\omega,t)+iF_I(\omega,t), \tag{28}$$

where, the real part and imaginary part of $F(\omega,t)$, $F_R(\omega,t)$ and $F_I(\omega,t)$, are given by

$$F_\Theta(\omega,t)=\frac{1}{2\pi}\int_{-\infty}^{+\infty}J_\varsigma\left(\omega'\right)\lambda_\Theta\left(\omega'+\omega,t\right)d\omega', \tag{29}$$

where, $\Theta=R$ and I, and $\lambda_R(\omega,t)=\sin(\omega t)/\omega$ and $\lambda_I(\omega,t)=[1-\cos(\omega t)]/\omega$ are the real part and imaginary part of $\lambda(\omega,t)$ given by

$$\lambda(\omega,t)=\int_0^t e^{i\omega\tau}d\tau. \tag{30}$$

Substituting Eq. (28) into Eq. (27) we obtain

$$\mathcal{D}^I_{mn,m'n'} = \mathcal{R}_{mn,m'n'} + i\mathcal{B}_{mn,m'n'}, \tag{31}$$

where, $\mathcal{R}_{mn,m'n'}$, which we call damping rate matrix element, is the rate matrix element related to the change of density matrix from the value of $\rho_{m'n'}$ to the value of ρ_{mn}[54]

$$\begin{aligned}\mathcal{R}_{mn,m'n'}(t) &= \frac{1}{\hbar^2}\Bigg\{-\delta_{nn'}\sum_k X_{mk}X_{km'}F_R(\omega_{km'},t) \\ &\quad + X_{mm'}X_{n'n}\left[F_R(\omega_{nn'},t)+F_R(\omega_{mm'},t)\right] \\ &\quad - \delta_{mm'}\sum_k X_{n'k}X_{kn}F_R(\omega_{kn'},t)\Bigg\},\end{aligned} \tag{32}$$

and $\mathcal{B}_{mn,m'n'}$ is the Lamb shift matrix element which leads to Lamb shifts of unperturbed energy levels[52,53]

$$\begin{aligned}\mathcal{B}_{mn,m'n'}(t) &= \frac{1}{\hbar^2}\Bigg\{\delta_{nn'}\sum_k X_{mk}X_{km'}F_I(\omega_{km'},t) \\ &\quad + X_{mm'}X_{n'n}\left[F_I(\omega_{nn'},t)-F_I(\omega_{mm'},t)\right] \\ &\quad - \delta_{mm'}\sum_k X_{n'k}X_{kn}F_I(\omega_{kn'},t)\Bigg\}.\end{aligned} \tag{33}$$

They satisfy the symmetric relations

$$\mathcal{R}_{nm,n'm'}(t) = \mathcal{R}_{mn,m'n'}(t), \tag{34}$$

and

$$\mathcal{B}_{nm,n'm'}(t) = -\mathcal{B}_{mn,m'n'}(t). \tag{35}$$

From Eq. (35) $\mathcal{B}_{mm,nn}(t) = 0$.

B. Steady Lamb shift matrix and damping rate matrix at a long time limit

In general, the damping rate matrix and Lamb shift matrix are time-dependent because both $F_R(\omega,t)$ and $F_I(\omega,t)$ depend on time. However, in the investigation of decoherence of a qubit, one is only interested in the behavior of the qubit after a sufficiently long time. In this case, the damping rate matrix and Lamb shift matrix can be well approximated by steady ones.

In fact, the autocorrelation function of a thermal bath impacts the system only in some time interval t_c which is called the correlation time[52]. As long as the upper limit in the integral of Eq. (30) $t \gg t_c$ it may be extended to the infinity with very little error.

Applying the integral

$$\int_0^\infty e^{\pm i\omega\tau}d\tau = \pi\delta(\omega) \pm i\mathcal{P}\frac{1}{\omega}, \tag{36}$$

where $\mathcal{P}$ represents the Cauchy principal value of the integral, to Eq. (30) one has

$$\lambda_R(\omega,\infty) = \pi\delta(\omega), \tag{37}$$

$$\lambda_I(\omega,\infty) = \mathcal{P}\frac{1}{\omega}. \tag{38}$$

Substituting Eqs. (37) and (38) into Eq. (29), one obtains

$$f_R(\omega) = F_R(\omega,\infty) = \frac{1}{2}J_\varsigma(-\omega), \tag{39}$$

$$f_I(\omega) = F_I(\omega,\infty) = \frac{1}{2\pi}\mathcal{P}\int_{-\infty}^{+\infty}\frac{J_\varsigma(\omega')}{\omega'+\omega}d\omega'. \tag{40}$$

In Eqs. (32) and (33), replacing F_R with f_R and F_I with f_I, we obtain steady damping rate matrix element $R_{mn,m'n'}$ and Lamb shift matrix element $B_{mn,m'n'}$. They are given by

$$\begin{aligned} R_{mn,m'n'} = \frac{1}{\hbar^2}\Bigg[&-\delta_{nn'}\sum_k X_{mk}X_{km'}f_R(\omega_{km'}) \\ &+X_{mm'}X_{n'n}\left[f_R(\omega_{nn'})+f_R(\omega_{mm'})\right] \\ &-\delta_{mm'}\sum_k X_{n'k}X_{kn}f_R(\omega_{kn'})\Bigg], \end{aligned} \tag{41}$$

and

$$\begin{aligned} B_{mn,m'n'} = \frac{1}{\hbar^2}\Bigg[&\delta_{nn'}\sum_k X_{mk}X_{km'}f_I(\omega_{km'}) \\ &+X_{mm'}X_{n'n}\left[f_I(\omega_{nn'})-f_I(\omega_{mm'})\right] \\ &-\delta_{mm'}\sum_k X_{n'k}X_{kn}f_I(\omega_{kn'})\Bigg], \end{aligned} \tag{42}$$

respectively. The $R_{mn,m'n'}$ and $B_{mn,m'n'}$ have the same symmetric relations as $\mathcal{R}_{mn,m'n'}$ and $\mathcal{B}_{mn,m'n'}$ given by Eqs. (34) and (35).

It is shown from Eq. (31) that the thermal bath affects the system via the damping rate matrix and Lamb shift matrix. The damping rate matrix elements represent decay rates in special cases. For instance, $R_{mm,mm}$ characterizes the rate of population change in the state m, $R_{nn,mm}$ describes the rate of population transfer from the states m to n, and $R_{mn,mn}$ represents the dephasing (coherence decay between the states m to n) rate of the off-diagonal elements of ρ_{mn}. In contrast, the Lamb shift matrix element such as $B_{mn,mm}$ represents the well-known Lamb shift of the state m induced by the thermal bath. Hence, the damping rate matrix makes the system relax and

decohere while the Lamb shift matrix makes the energy levels shift. In addition, the symmetries of the Lamb shift matrix given by Eq. (35) are the same as those of the matrix for driving fields given by Eq. (21). In particular, when substituting Eq. (31) into Eq. (15) the Lamb shift matrix can be incorporated into the matrix $\mathcal{L}^F_{mn,m'n'}$ and leads to the renormalization of the quantum system Hamiltonian.[53] Thus the effect of the Lamb shift matrix is analogous to an extra field. In the case of weak damping, the Lamb shift matrix is very small compared to the driving field and thus is neglected hereafter.

C. Spectral density, spontaneous decay, stimulated transition, and detailed balance

The fluctuation of the thermal bath at temperature T is characterized by a spectral density. The spectral density is computed from the real part of the frequency-dependent damping coefficient $\gamma_R(\omega)$ in terms of the quantum fluctuation-dissipation theorem (see the Appendix B for details).[47,48] For the interaction given by Eq. (6), the fluctuation force $\xi(t)$ is proportional to the fluctuation force $\varsigma(t)$ by

$$\xi(t) = \Lambda\varsigma(t), \tag{43}$$

where,

$$\Lambda = -\frac{\partial X}{\partial q}, \tag{44}$$

and q is the coordinate operator of the system. For the weak damping considered here the interaction given by Eq. (6) is a linear function of system coordinate operator and thus Λ is a constant.

For the thermal bath at temperature T, the spectral density $J_\xi(\omega)$ of the fluctuation force $\xi(t)$ is given by Eq. (B3). From Eqs. (B3) and (43), the spectral density $J_\varsigma(\omega)$ of the fluctuation force $\varsigma(t)$ is given by

$$J_\varsigma(\omega) = \frac{J_\xi(\omega)}{\Lambda^2} = \frac{M\hbar\omega}{\Lambda^2}\gamma_R(\omega)\left[1+\coth\left(\frac{\hbar\omega}{2k_BT}\right)\right]. \tag{45}$$

Substituting Eq. (45) into Eq. (12), we obtain the autocorrelation function of the fluctuation force $\varsigma(t)$

$$\begin{aligned}\mathcal{J}(t) &= \frac{M\hbar}{2\pi\Lambda^2}\int_{-\infty}^{+\infty}\omega\gamma_R(\omega)\left[1+\coth\left(\frac{\hbar\omega}{2k_BT}\right)\right]\\ &\quad\times\exp(i\omega t)\,d\omega.\end{aligned} \tag{46}$$

In general, the autocorrelation function given by Eq. (46) is complex and irreversible since the integrand does not have a definite symmetry with respect to ω. This result is totally different from that for a classical system, for which the autocorrelation function is real and reversible. As has been demonstrated, the irreversibility of the autocorrelation function results from the non-Hermitian property and noncommutable property of the thermal bath operators.

Substituting Eqs. (45) and (39) into Eq. (41), we obtain for $m \neq n$ the rate of population transfer from the state n to m

$$\begin{aligned} R_{mm,nn} &= -\frac{M\left|X_{mn}\right|^2}{\hbar\Lambda^2}\omega_{mn}\gamma_R(-\omega_{mn}) \\ &\quad \times\left[1-\coth\left(\frac{\hbar\omega_{mn}}{2k_BT}\right)\right]. \end{aligned} \tag{47}$$

From Eqs. (41) and (47) we also obtain the rate of population change in the state n

$$R_{nn,nn} = -\sum_{m(\neq n)} R_{mm,nn}. \tag{48}$$

This indicates that $R_{nn,nn}$ is a sum of the rates of population transfer from the state n to all the other states m. This result is identical with that of atomic systems.[52]

1. *Spontaneous decay*

Let us consider a pair of states denoted by m and n. Suppose the state m has lower energy than the state n. The transition frequency is $\omega_{nm} = (E_n - E_m)/\hbar > 0$. If the system is in the higher energy state initially, it can decay without presence of any external field due to the stimulation of thermal fluctuation of the thermal bath. This process is the so-called spontaneous decay. During this process the system transits from the higher energy state n to the lower energy state m with emission of radiation. From Eq. (47) the spontaneous decay rate Γ_{mn}^{SP} is given by

$$\begin{aligned} \Gamma_{mn}^{SP} &= \frac{M\left|X_{mn}\right|^2}{\hbar\Lambda^2}\omega_{nm}\gamma_R(\omega_{nm}) \\ &\quad \times\left[1+\coth\left(\frac{\hbar\omega_{nm}}{2k_BT}\right)\right]. \end{aligned} \tag{49}$$

It is proportional to the transition matrix element X_{mn}, energy level spacing ω_{nm}, and damping coefficient $\gamma_R(\omega_{nm})$. It also depends on the temperature via the factor $\coth(\hbar\omega_{nm}/2k_BT)$.

2. *Stimulated transition*

If the system is in the lower energy state initially it may occur an inverse process with respect to the spontaneous decay under the stimulation of thermal fluctuation, making the system transit

from the lower energy state m to the higher energy state n. This process is the so-called stimulated transition. From Eq. (47) the stimulated transition rate Γ_{nm}^{ST} is given by

$$\begin{aligned}\Gamma_{nm}^{ST} &= -\frac{M\left|X_{mn}\right|^2}{\hbar\Lambda^2}\omega_{nm}\gamma_R(-\omega_{nm}) \\ &\times\left[1-\coth\left(\frac{\hbar\omega_{nm}}{2k_BT}\right)\right].\end{aligned} \tag{50}$$

3. Detailed balance

In general, $\gamma_R(\omega)$ is an even function of ω, i.e., $\gamma_R(-\omega)=\gamma_R(\omega)$. Using Eqs. (49) and (50) one has

$$\frac{\Gamma_{mn}^{SP}}{\Gamma_{nm}^{ST}}=\exp\left(\frac{E_n-E_m}{k_BT}\right). \tag{51}$$

Thus the ratio of the spontaneous decay rate to the stimulated transition rate satisfies the detailed balance principle.

V. DECOHERENCE OF A DISSIPATIVE TWO-LEVEL SYSTEM

An ideal qubit is a two-level system and an ideal qubit interacting with a thermal bath is equivalent to a dissipative two-level system (DTLS). For a DTLS, the master equation (15) can be replaced by the Bloch equation.[57] In the rotating-wave approximation (RWA), analytical solutions of the Bloch equation can be obtained, from which analytical expressions of characteristic (relaxation, decoherence, and dephasing) times of the DTLS can be derived. In this section, we present some important analytical results without derivation. The details about these analytical results can be found in our previous paper.[57]

A. Relaxation and decoherence times of the DTLS in the absence of driving fields

In the absence of driving fields, the relaxation and decoherence times of the DTLS are given by

$$T_1=\kappa_1^{-1}, \tag{52}$$

and

$$T_2=\kappa_2^{-1}, \tag{53}$$

respectively, where, κ_1 is the relaxation rate of the DTLS in free decay given by

$$\kappa_1=R_{22,11}+R_{11,22}, \tag{54}$$

and κ_2 is the decoherence rate of the the DTLS in free decay given by

$$\kappa_2 = -R_{12,12}. \tag{55}$$

These results accord with those obtained by others.[21] In general, due to dephasing $T_2 < 2T_1$.[35] The dephasing time T_φ can be calculated from T_1 and T_2 by[21]

$$\frac{1}{T_\varphi} = \frac{1}{T_2} - \frac{1}{2T_1}. \tag{56}$$

B. Relaxation and decoherence times of the DTLS in the presence of a resonant ac driving field

For an DTLS resonantly driven by an ac field, multiple relaxation and decoherence times are required to completely describe time evolution of population and coherence of the qubit.[57] Particularly, intrinsic and field-induced decoherence times are necessitated to characterize the decoherence. In the underdamped regime, the most important regime for the driven qubit, the relaxation time $\widetilde{T}_1$ is given by

$$\widetilde{T}_1 = \Gamma^{-1}, \tag{57}$$

where, the tilt "$\sim$" is used to denote the characteristic times of the resonantly driven qubit and Γ is the relaxation rate of the driven DTLS given by

$$\Gamma = \frac{\kappa_1 + \kappa_2}{2}. \tag{58}$$

The intrinsic decoherence time $\widetilde{T}_{21}$ and field-induced decoherence time $\widetilde{T}_{22}$ are given by

$$\widetilde{T}_{21} = \kappa_2^{-1} = T_2, \tag{59}$$

and

$$\widetilde{T}_{22} = \Gamma^{-1} = \widetilde{T}_1, \tag{60}$$

respectively. It is shown that due to the effect of driving fields the characteristic times of the driven DTLS are different from those of the DTLS in free decay. The characteristic times of the driven DTLS are independent of the field strength in the case of weak driving fields. If the initial state of the driven DTLS is an eigenstate such as the ground state, the intrinsic decoherence vanishes and the decoherence is completely characterized by the field-induced decoherence. In this case, the decoherence rate of the driven DTLS is equal to its relaxation rate as shown by Eq. (60).

Therefore, the escape rate of quantum phase information from the system equals to the rate of energy flowing from the system to the environment. This result is identical with that obtained from the non-Markovian approach with inclusion of both bath and qubit dynamics.[27]

From Eqs. (52), (53), (59), and (60) we obtain

$$\frac{1}{\widetilde{T}_{22}} = \frac{1}{\widetilde{T}_1} = \frac{1}{2T_1} + \frac{1}{2T_2} = \frac{3}{4T_1} + \frac{1}{2T_\varphi}. \tag{61}$$

It shown that $\widetilde{T}_{22} = \widetilde{T}_1$, $\min(T_1, T_2) \leq \widetilde{T}_1\left(\widetilde{T}_{22}\right) \leq \max(T_1, T_2)$, and $\widetilde{T}_1\left(\widetilde{T}_{22}\right) < \min(4T_1/3, 2T_\varphi)$. These results are similar to those obtained by others[28,58] and also agrees, within the experimental uncertainties, with recent experimental results.[20]

VI. DECOHERENCE OF A 2D SQUID FLUX QUBIT COUPLED TO CONTROL AND READOUT CIRCUITS

A number of effects can destroy coherence of a SQUID qubit,[59] of which the fluctuation of external circuits used for control and readout of the qubit is one of the important sources of decoherence.[17] In this section, we investigate decoherence of a 2D SQUID flux qubit due to coupling with control and readout circuits and effect of driving fields on the decoherence.

A. Hamiltonian of the microwave-driven 2D SQUID flux qubit

As shown in FIG. 1, a 2D SQUID flux qubit is a variable barrier rf SQUID in which the single Josephson junction in an ordinary rf SQUID is replaced by a low inductance dc SQUID.[39] Suppose that the inductance of the superconducting loop of the rf SQUID is L, the critical current is I_c, the total magnetic flux enclosed in the rf SQUID loop is Φ, the shunt capacitance of each Josephson junction in the dc SQUID is C, the critical currents are I_{c1} and I_{c2}, and the total magnetic flux enclosed in the dc SQUID loop is Φ_{dc}. The Hamiltonian of the 2D SQUID qubit can be written as

$$H_S(x, y) = \frac{p_x^2}{2m_x} + \frac{p_y^2}{2m_y} + V(x, y), \tag{62}$$

where, $m_x = 2C\Phi_0^2$ and $m_y = C\Phi_0^2/2$ are the masses of the first and second modes, $\Phi_0 \equiv h/2e$ and e are the flux quantum and elementary charge, $x = \Phi/\Phi_0$ and $y = \Phi_{dc}/\Phi_0$ are the canonical coordinates of the 2D SQUID qubit, $p_x = -i\hbar\partial/\partial x$ and $p_y = -i\hbar\partial/\partial y$ are the canonical momenta

conjugate to x and y, and $V(x,y)$ is the potential energy given by[60]

$$V(x,y) = \frac{\Phi_0^2}{L}\left[\frac{1}{2}(x-x_e)^2+\frac{g}{2}(y-y_e)^2 - \frac{\beta_L}{4\pi^2}\cos(2\pi x)\cos(\pi y) + \frac{\delta\beta_L}{4\pi^2}\sin(2\pi x)\sin(\pi y)\right]. \quad (63)$$

Here, $g \equiv L/2l$ is the ratio of the inductances of the rf SQUID and dc SQUID, $\beta_L \equiv 2\pi L I_c/\Phi_0$, $\delta\beta_L \equiv 2\pi L(I_{c2}-I_{c1})/\Phi_0$, x_e and y_e are the fluxes applied to the rf SQUID and dc SQUID in the unit of Φ_0. The Josephson coupling energy of the rf SQUID is $E_J = \hbar I_c/2e = m\omega_{LC}^2\beta_L/4\pi^2$, where $\omega_{LC} = 1/\sqrt{LC}$ is the characteristic frequency of the 2D SQUID qubit. The contour of the potential energy of the 2D SQUID qubit used in recent experiment[39] is plotted in FIG. 2, where the parameters of the 2D SQUID qubit are $L = 205$ pH, $C = 32.5$ fF, $g = 17.0$, $\beta_L = 3.7$, $\delta\beta_L = 0$, $x_e = 0.4991$, and $y_e = 0.387$.

The spectroscopic properties of the 2D SQUID qubit can be obtained by solving the eigenvalue equation of Hamiltonian H_S.[15,18] In FIG. 3 and FIG. 4, we plot the energy levels and transition matrix elements versus the flux applied to the rf SQUID x_e, respectively. When $x_e = 0.4991$, at the position of the arrow, $\Delta E_{31} = E_3 - E_1 = 0.259\omega_{LC} = 15.95$ GHz and $|x_{21}/x_{32}| = 0.262$, where $\omega_{LC} = 3.874\times10^{11}$ rad/s. These results are in very good agreement with the experimental results.[39] Note that x_e and y_e determine the energy bias and tunnel splitting, respectively. Thus the spectroscopic properties of the 2D SQUID qubit can be varied *in situ* by adjusting x_e and y_e.

In order to manipulate the qubit's states for gate operations, a microwave pulse is applied to the 2D SQUID qubit through the first mode. If the interaction of the microwave field and external circuits is neglected, the Hamiltonian of the microwave-driven 2D SQUID qubit coupled to the external circuits is given by

$$H(x,t) = H_S(x,y) + H_F(x,t) + H_I(x,y,t), \quad (64)$$

where, $H_F(x,t)$ is the interaction of the SQUID qubit and the microwave field and $H_I(x,y,t)$ is the interaction of the SQUID qubit and the external circuits (thermal bath).

If $\phi(t)$ is the normalized flux from the microwave field coupled to the SQUID qubit, which is taken to be

$$\phi(t) = \phi_\mu\cos(\omega_\mu t), \quad (65)$$

where, ϕ_μ and ω_μ are the field strength and frequency, respectively, then $H_F(x,t)$ is given by[15]

$$H_F(x,t) = \frac{\Phi_0^2}{2L}\phi\left[\phi - 2(x-x_e)\right]. \quad (66)$$

In general, the external circuits are coupled to the 2D SQUID qubit through both modes. However, the coupling through the second mode is negligibly small compared to that through the first mode and will be neglected. In the case of weak coupling, the interaction of the 2D SQUID qubit and the external circuits is a linear function of x and can be expressed by[17,34]

$$H_I(x,t) = x\varsigma\left(t\right), \tag{67}$$

where, $\varsigma\left(t\right)$ is the fluctuation force of the external circuits. If the coupling between the control and readout circuits is neglected, $\varsigma\left(t\right)$ can be decomposed into two parts as

$$\varsigma\left(t\right) = \varsigma_x\left(t\right) + \varsigma_m(t), \tag{68}$$

where, $\varsigma_x\left(t\right)$ and $\varsigma_m(t)$ are the fluctuation forces of the control and readout circuits, respectively.

B. Spectral densities of the control and readout circuits

As has been demonstrated, in the case of weak damping, the effect of a thermal bath on a quantum system can be characterized by a spectral density.[46,48] The spectral density can be computed from the frequency-dependent damping coefficient of the quantum Langevin equation (see Appendix B). For the 2D SQUID flux qubit, the quantum Langevin equation is given by[48]

$$C\frac{d^2\Phi(t)}{dt^2} + \int_{t_0}^{t} dt' Y\left(t-t'\right)\frac{d\Phi(t')}{dt'} + \frac{dV\left(\Phi\right)}{d\Phi} = \xi_\Phi\left(t\right), \tag{69}$$

where, the damping coefficient $Y(t)$ is the equivalent admittance of the external circuits, $V\left(\Phi\right)$ is the potential energy applied to the SQUID qubit, and $\xi_\Phi\left(t\right)$ is the fluctuation force of the external circuits.

By comparison of Eq. (69) with Eq. (B1), one has $q \to \Phi$, $M \to C$, $\gamma \to Y/C$, and $\xi \to \xi_\Phi$. Applying these relations to Eq. (B3), we obtain the spectral density $J\left(\omega\right)$ of the fluctuation force $\xi_\Phi\left(t\right)$

$$J\left(\omega\right) = \hbar\omega Y_R(\omega)\left[1 + \coth\left(\frac{\hbar\omega}{2k_BT}\right)\right], \tag{70}$$

where, T is the temperature of the external circuits and $Y_R(\omega)$ is the real part of the frequency-dependent equivalent admittance $Y(\omega)$ of the external circuits. $Y(\omega)$ can be calculated from $Y(t)$ by Fourier transform. It can also be calculated directly from the external circuits using circuit equations in the frequency domain. For the control and readout circuits given in FIG. 1, $Y(\omega)$ has been derived (see Appendix C for details) and $Y_R(\omega)$ is given by

$$Y_R(\omega) = Y_{xR}(\omega) + Y_{mR}(\omega), \tag{71}$$

where, $Y_{xR}(\omega)$ and $Y_{mR}(\omega)$ are the real parts of the frequency-dependent admittances of the control circuit and readout circuit, respectively. They are given by

$$Y_{xR}(\omega) = \frac{F_x(\omega)}{\omega^2 + G_x(\omega)}, \tag{72}$$

and

$$Y_{mR}(\omega) = \frac{1}{F_m(\omega)\left[1 + G_m(\omega)\omega^2\right]}, \tag{73}$$

respectively, where, $F_x(\omega)$, $G_x(\omega)$, $F_m(\omega)$, and $G_m(\omega)$ are given by Eqs. (C8), (C9), (C22), and (C23) in Appendix C. Substituting Eq. (71) into Eq. (70), one has

$$J(\omega) = J_x(\omega) + J_m(\omega), \tag{74}$$

where, $J_x(\omega)$ and $J_m(\omega)$ are the spectral densities of the control circuit and readout circuit, respectively. They can be calculated using Eq. (70) with $Y_R(\omega)$ replaced by $Y_{xR}(\omega)$ and $Y_{mR}(\omega)$, respectively.

In FIG. 5 we plot the spectral densities $J_x(\omega)$, $J_m(\omega)$, and $J(\omega)$ versus the frequency ω for the control and readout circuits of the 2D SQUID qubit used in the experiment.[39] The parameters of the control circuit are $L_x = 100$ pH, $C_x = 25$ pF, $R_x = 70\ \Omega$, and $R_{x0} = 1.0 \times 10^3\ \Omega$. The parameters of the readout circuit are $L_{10} = L_{20} = 20$ pH, $L_{J1} = 100$ pH, $L_{J2} = 550$ pH, $C_m = 20$ pF, $R_m = 70\ \Omega$, and $R_{m0} = 2.0 \times 10^4\ \Omega$. The mutual inductances $M_x = 1.0$ pH and $M_m = 3.3$ pH, and the temperature $T = 30$ mK. It is shown that the spectral density $J(\omega)$ (also $J_x(\omega)$ and $J_m(\omega)$) reaches the maximum at $\omega \simeq 1.69\omega_{LC}$. At low frequency, the spectral density $J(\omega)$ (also $J_x(\omega)$ and $J_m(\omega)$) approaches a constant value, in particular $J(0) \neq 0$. As will be demonstrated, the dephasing time T_φ is finite if $J(0) \neq 0$. Thus the control and readout circuits of the 2D SQUID qubit induce both relaxation and dephasing.

C. Damping rate matrix

From Eq. (67), the fluctuation force $\xi_\Phi(t)$ is given by

$$\xi_\Phi(t) = -\frac{\partial H_I(x,t)}{\partial \Phi} = -\frac{1}{\Phi_0}\varsigma(t). \tag{75}$$

This equation provides a relation between the fluctuation force $\varsigma(t)$ and $\xi_\Phi(t)$ of the external circuits. Compared Eq. (75) with Eq. (43), one has $\Lambda = -1/\Phi_0$. Using Eq. (45), the spectral

density $J_\varsigma(\omega)$ of the fluctuation force $\varsigma(t)$ can be calculated from the spectral density $J(\omega)$ of the fluctuation force $\xi_\Phi(t)$ by

$$J_\varsigma(\omega) = \Phi_0^2 J(\omega). \tag{76}$$

For the 2D SQUID qubit, $X_1 = x$ and $X_2 = y$. Substituting Eqs. (39) and (76) into Eq. (41) we obtain the steady damping rate matrix element $R_{mn,m'n'}$ of the 2D SQUID qubit

$$\begin{aligned} R_{mn,m'n'} &= \frac{\Phi_0^2}{2\hbar^2}\Bigg[-\delta_{nn'}\sum_k x_{mk}x_{km'}J(\omega_{m'k}) \\ &\quad + x_{mm'}x_{n'n}\left[J(\omega_{n'n}) + J(\omega_{m'm})\right] \\ &\quad - \delta_{mm'}\sum_k x_{n'k}x_{kn}J(\omega_{n'k})\Bigg]. \end{aligned} \tag{77}$$

It is a function of transition matrix elements and spectral densities.

If only considering the two computational levels, the 2D SQUID qubit is equivalent to a DTLS and its characteristic (relaxation, decoherence, and dephasing) times can be calculated analytically. Substituting Eq. (77) into Eqs. (54) and (55), then Eqs. (54) and (55) into Eqs. (52), (53), and (56), one has

$$T_1^{-1} = \frac{\pi^2}{e^2}|x_{12}|^2\left[J(\omega_{21}) + J(\omega_{12})\right], \tag{78}$$

$$T_2^{-1} = \frac{1}{2T_1} + \frac{\pi^2}{2e^2}(x_{11} - x_{22})^2 J(0), \tag{79}$$

and

$$T_\varphi^{-1} = \frac{\pi^2}{2e^2}(x_{11} - x_{22})^2 J(0). \tag{80}$$

It is shown that the relaxation and dephasing rates are determined by the spectral densities at transition frequency $\omega = |\omega_{21}|$ and low frequency $\omega = 0$, respectively.[20,21,24,34,40,41] The relaxation rate is proportional to the modulus square of transition matrix element $|x_{12}|^2$, while the dephasing rate is proportional to the squared difference of average coordinates of the two states $(x_{11} - x_{22})^2$. For a qubit having $(x_{11} - x_{22}) = 0$, the dephasing is completely suppressed. For the 2D SQUID qubit considered here, both $J(0)$ and $(x_{11} - x_{22})^2$ are not zero. Thus the control and readout circuits will induce phase relaxation.

For the 2D SQUID flux qubit, $Y_{xR}(\omega)$, $Y_{mR}(\omega)$, and thus $Y_R(\omega)$ are even functions of ω. Substituting Eq. (70) into Eqs. (78) to (80), the analytical expressions of the characteristic times

are simplified to

$$T_1^{-1} = \frac{2\pi^2}{e^2}\hbar\omega_{21}\left|x_{12}\right|^2 Y_R\left(\omega_{21}\right)\coth\left(\frac{\hbar\omega_{21}}{2k_BT}\right), \tag{81}$$

$$T_2^{-1} = \frac{1}{2T_1} + \frac{\pi^2}{e^2}k_BT\left(x_{11}-x_{22}\right)^2 Y_R\left(0\right), \tag{82}$$

and

$$T_\varphi^{-1} = \frac{\pi^2}{e^2}k_BT\left(x_{11}-x_{22}\right)^2 Y_R\left(0\right). \tag{83}$$

Now the relaxation rate is dominated by the external circuits' admittance at transition frequency ω_{21} while the dephasing rate by the admittance at $\omega = 0$. Furthermore, the dephasing rate is proportional to the temperature of the thermal bath. Hence at low temperature the dominating source of decoherence is relaxation while at high temperature the main source of decoherence is dephasing. These results agree with those obtained by others.[21,33,46]

Using Eq. (49), the general form of spontaneous decay rate, we obtain the spontaneous decay rate of the 2D SQUID flux qubit

$$\begin{aligned}\Gamma_{mn}^{SP} &= \frac{2\pi}{\hbar}R_Q\left|x_{mn}\right|^2\left(E_n-E_m\right)Y_R(\omega_{nm}) \\ &\quad\times\left[1+\coth\left(\frac{E_n-E_m}{2k_BT}\right)\right],\end{aligned} \tag{84}$$

where, $R_Q = h/4e^2$ is the resistance quantum and $\omega_{nm} = \left(E_n - E_m\right)/\hbar > 0$. If the equivalent impedance is a resistance R, then $Y_R(\omega_{nm}) = 1/R$ and the spontaneous decay rate is the same as that given by others with different method.[61,62]

D. Numerical method

In the Hilbert space spanned by the eigenstates of the qubit's Hamiltonian, the density matrix is governed by the master equation (15). This equation can be rewritten in matrix form as

$$\frac{d\boldsymbol{\rho}}{dt} = -i\mathbf{L}\boldsymbol{\rho} + \mathbf{R}\boldsymbol{\rho}, \tag{85}$$

where, $\boldsymbol{\rho} = \left\{\rho_\mu\right\}$ is the density matrix, $\mathbf{L} = \left\{\mathcal{L}_{\mu\mu'}^S + \mathcal{L}_{\mu\mu'}^F\right\}$ is the matrix of Liouville superoperators, $\mathbf{R} = \left\{R_{\mu\mu'}\right\}$ is the damping rate matrix, $\mu = mn$, and $\mu' = m'n'$. In Eq. (85) the Lamb shift matrix has been neglected. The matrix $\mathbf{L}$ is a time-independent, real, and symmetric matrix. Its matrix elements are given by Eqs. (18) and (19). The matrix $\mathbf{R}$ is also a time-independent and real but non-symmetric matrix. Its matrix elements are given by Eq. (77).

To solve Eq. (85), we use the split-operator method.[63] Using this method, the propagation of the density matrix is calculated by

$$\boldsymbol{\rho}\left(t+\Delta t\right)=\mathbf{P}_{L}\left(t\right)\mathbf{P}_{R}\left(t\right)\mathbf{P}_{L}\left(t\right)\boldsymbol{\rho}\left(t\right), \tag{86}$$

where, $\mathbf{P}_{L}\left(t\right)$ and $\mathbf{P}_{R}\left(t\right)$ are the propagators. They are given by

$$\mathbf{P}_{\Theta}\left(t\right)=\exp\left(\lambda\mathbf{Q}\Delta t\right), \tag{87}$$

where, $\lambda=-i/2$ and $\mathbf{Q}=\mathbf{L}\left(t+\Delta t/2\right)$ for $\Theta=L$, and $\lambda=1$ and $\mathbf{Q}=\mathbf{R}\left(t+\Delta t/2\right)$ for $\Theta=R$.

Suppose that $\mathbf{Q}$ is an $N\times N$ matrix, and its eigenvalue and right eigenvector are q_k and $B_k=\left[b_{1k},b_{2k},\cdots,b_{Nk}\right]^{T}$, respectively, where T denotes the transpose of the vector. We assume that $\mathbf{q}=\{q_k\delta_{k'k}\}$ and $\mathbf{B}=\{b_{k'k}\}$ are the two matrices constructed respectively by the eigenvalue q_k and eigenvector B_k, then the matrix $\mathbf{Q}$ can be calculated by

$$\mathbf{Q}=\mathbf{B}\mathbf{q}\mathbf{B}^{-1}, \tag{88}$$

where, $\mathbf{B}^{-1}$ is the inverse matrix of $\mathbf{B}$. Substituting Eq. (88) into Eq. (87), the propagator $\mathbf{P}_{\Theta}\left(t\right)$ is then given by

$$\mathbf{P}_{\Theta}\left(t\right)=\mathbf{B}\exp\left(\lambda\mathbf{q}\Delta t\right)\mathbf{B}^{-1}, \tag{89}$$

where, $\exp\left(\lambda\mathbf{q}\Delta t\right)$ is a diagonal matrix with non-zero diagonal matrix elements given by $\exp\left(\lambda q_k\Delta t\right)$. If $\mathbf{Q}$ is a Hermitian operator $\mathbf{B}^{-1}=\mathbf{B}^{\dagger}$ and if $\mathbf{Q}$ is a real and symmetric operator (e.g., $\mathbf{L}$) $\mathbf{B}^{-1}=\mathbf{B}^{T}$.

E. Effect of driving fields on relaxation and decoherence times

By numerically solving the master equation in terms of the numerical method introduced in the preceding section, population and coherence of the microwave-driven 2D SQUID qubit are calculated, from which the relaxation and decoherence times are extracted.

1. Free decay of the 2D SQUID qubit

To numerically calculate the relaxation and decoherence times of the 2D SQUID qubit in the absence of driving fields (free decay) we assume that the initial state of the qubit is a superposition state of the two computational states $|1\rangle$ and $|2\rangle$ with $\rho_{11}\left(0\right)=\rho_{12}\left(0\right)=\rho_{21}\left(0\right)=\rho_{22}\left(0\right)=0.5$

and $\rho_{ij}(0) = 0$ for all the other combination of i and j. To take into account the leakage to non-computational states we include four levels ($N = 4$) in the calculation. In the case of weak driving fields and weak damping, the calculation with four levels ($N = 4$) is converged. By numerically solving the master equation (85) with the aforementioned initial state we obtain the population and coherence of the 2D SQUID qubit in free decay. Since the coherence is usually a complex and fast oscillating, we use $|\rho_{12}|^2$ instead of ρ_{12} to estimate the decoherence time. In FIG. 6 and FIG. 7, we show with the solid lines the evolution of population inversion ($\rho_{22} - \rho_{11}$) and the squared modulus of coherence $|\rho_{12}|^2$, respectively.

For the DTLS, the population inversion and squared modulus of coherence in free decay undergo simple exponential decays with[57]

$$\rho_{22} - \rho_{11} = y_1 + z_1 e^{-t/\tau_1}, \tag{90}$$

and

$$|\rho_{12}|^2 = y_2 + z_2 e^{-2t/\tau_2}, \tag{91}$$

where, the parameters τ_1 and τ_2 are the relaxation and decoherence times of the DTLS in free decay, respectively.

To calculate the relaxation and decoherence times of the 2D SQUID qubit in free decay, we fit the numerical results of ($\rho_{22} - \rho_{11}$) and $|\rho_{12}|^2$ to the above exponential functions. The results of least-square fitting are plotted in FIG. 6 and FIG. 7 with the dashed lines, from which we obtain $T_1 = \tau_1 = 3.429$ μs and $T_2 = \tau_2 = 2.243$ μs. The calculated relaxation time is in very good agreement with the experimental result $T_1 = 3.45$ μs,[39] demonstrating the validity of our approach and calculation. Using Eq. (56), we obtain the dephasing time $T_\varphi = 3.333$ μs. For comparison, we also calculate the relaxation and decoherence times using the analytical expressions of the DTLS in free decay given by Eqs. (81) to (83). The results $T_1 = 3.429$ μs, $T_2 = 2.243$ μs, and $T_\varphi = 3.333$ μs are exactly same as the numerical results. In addition, since the decoherence time is shorter than the relaxation time the dephasing is the main source of decoherence.

2. Rabi oscillation of the resonantly driven 2D SQUID qubit

To calculate the relaxation and decoherence times of the 2D SQUID qubit in the presence of a microwave field, we assume that the initial state of the qubit is the ground state with $\rho_{11}(0) = 1$ and $\rho_{ij}(0) = 0$ for all the other i and j. By numerically solving the master equation (85) with this

initial condition, the population and coherence and thus the relaxation and decoherence times of the driven 2D SQUID qubit are calculated. The relaxation and decoherence times of the driven qubit depend on the relative value of the field strength to the damping strength.[57] In the underdamped regime for which the field strength is larger than the damping strength, the decoherence can be decomposed into intrinsic and field-induced ones. If the initial state of the qubit is the ground state, the intrinsic decoherence vanishes and the qubit has a single decoherence time which equals to the field-induced decoherence time.

In FIG. 8 and FIG. 9 we plot with the solid lines the evolution of population difference $(\rho_{11}-\rho_{22})$ and squared modulus of coherence $|\rho_{12}|^2$, respectively, for the 2D SQUID qubit resonantly driven by the microwave field with $\phi_\mu = 1.0\times 10^{-5}$ and $\omega_\mu = \omega_{21} = 0.127\omega_{LC}$. As shown in these figures, both $(\rho_{11}-\rho_{22})$ and $|\rho_{12}|^2$ undergo damped Rabi oscillations.

In the underdamped regime, the population difference and squared modulus of coherence of the resonantly driven DTLS from an eigenstate undergo damped Rabi oscillations as[57]

$$\rho_{11}-\rho_{22} = \widetilde{y}_1 + \widetilde{z}_1 \sin\left(\Omega t+\varphi_1\right) e^{-t/\widetilde{\tau}_1}, \tag{92}$$

and

$$\begin{aligned} |\rho_{12}|^2 \;=\; & \widetilde{y}_2 + \widetilde{z}_2 \sin\left(\Omega t+\varphi_2\right) e^{-t/\widetilde{\tau}_2} \\ & + \widetilde{z}_3 \sin^2\left(\Omega t+\varphi_2\right) e^{-2t/\widetilde{\tau}_2}, \end{aligned} \tag{93}$$

where, Ω is the Rabi frequency, and $\widetilde{\tau}_1$ and $\widetilde{\tau}_2$ are the relaxation and (field-induced) decoherence times of the driven DTLS, respectively.

To extract the relaxation and decoherence times of the driven 2D SQUID qubit, we fit the calculated $(\rho_{11}-\rho_{22})$ and $|\rho_{12}|^2$ to the aforementioned exponentially damped Rabi oscillating functions. The results of the best fit are shown in FIG. 8 and FIG. 9 with dashed lines, from which we obtain $\Omega = 4.016\times 10^{-5}\omega_{LC}$, $\widetilde{T}_1 = \widetilde{\tau}_1 = 2.689$ μs, and $\widetilde{T}_{22} = \widetilde{\tau}_2 = 2.682$ μs.

Using the same procedure, we have calculated the relaxation and decoherence times of the 2D SQUID qubit resonantly driven by the microwave fields with different field strengths. The results are given in the columns with $N=4$ in TABLE I. To examine the effect of leakage on the relaxation and decoherence times, we have also calculated the relaxation and decoherence times only using the two computational states. The results are given in the columns with $N=2$ in TABLE I. In the case of weak driving fields and weak damping, the 2D SQUID qubit may be well approximated by a DTLS. Form the analytical expressions of relaxation and decoherence times of the driven DTLS given by Eqs. (61), (81), and (82), we obtain $\widetilde{T}_1 = \widetilde{T}_{22} = 2.712$ μs. They are independent of driving field strength.

TABLE I shows that when $\phi_\mu \leq 1 \times 10^{-6}$ the calculated relaxation and decoherence times of the driven 2D SQUID qubit are essentially identical. They are independent of the driving field strengths, shorter than the relaxation time and longer than the decoherence time of the 2D SQUID qubit in free decay. These results accord with those obtained from the calculation with the analytical expressions of characteristic times of the driven DTLS. The relaxation and decoherence times obtained from the calculation with $N = 4$ are the same as those with $N = 2$ and those with the analytical expressions, demonstrating that both the strong field effect and leakage are negligibly small in this case. When $\phi_\mu \geq 5 \times 10^{-6}$, on one hand, the relaxation time obtained from the calculation with $N = 4$ equals to that with $N = 2$, indicating that the leakage does not influence the relaxation time. On the other hand, the relaxation time obtained from the calculation with $N = 2$ is less than that obtained from the calculation with the analytical expressions, illustrating that the strong field effect makes the relaxation time smaller. In contrast, due to the strong field effect the decoherence time obtained from the calculation with $N = 2$ increases slowly with the field strength, while due to the leakage the decoherence time obtained from the calculation with $N = 4$ decreases with the field strength quickly. In particular, when $\phi_\mu \geq 1 \times 10^{-4}$ the squared modulus of coherence obtained from the calculation with $N = 4$ no longer undergoes the simple damped Rabi oscillation as that given by Eq. (93). Thus the relaxation time is sensitive to the strong field effect while the decoherence time is sensitive to the leakage.

TABLE I: Numerical results of relaxation and decoherence times (μs) of the 2D SQUID qubit in free and driven decays.

Field strength	Relaxation time		Decoherence time	
	$N = 4$	$N = 2$	$N = 4$	$N = 2$
0	3.429	3.429	2.243	2.243
1×10^{-7}	2.712	2.712	2.712	2.712
5×10^{-7}	2.712	2.712	2.712	2.712
1×10^{-6}	2.712	2.712	2.712	2.712
5×10^{-6}	2.706	2.706	2.705	2.713
1×10^{-5}	2.689	2.689	2.682	2.716
5×10^{-5}	2.224	2.224	1.945	2.742
1×10^{-4}	1.480	1.480	–	2.837

F. Optimization of the control and readout circuits

The decoherence of the 2D SQUID qubit strongly depends on the control and readout circuits. To optimize the control and readout circuits for long decoherence time, we investigate how the characteristic times change with the parameters and temperature of the circuits of the 2D SQUID qubit in free and driven decays. The strength of the resonant microwave field used is $\phi_\mu = 1\times10^{-5}$.

1. Characteristic times versus mutual inductances

In FIG. 10 we show the characteristic times versus the mutual inductance M_x between the 2D SQUID qubit and the control circuit. In this figure, T_1 and T_2 are the relaxation and decoherence times of the qubit in free decay, and $\widetilde{T}_1$ and $\widetilde{T}_{22}$ are those of the qubit in driven decay. It is shown that for all the values of M_x shown in this figure $\widetilde{T}_1 \simeq \widetilde{T}_{22}$ and $\min(T_1,T_2) \lesssim \widetilde{T}_1 \lesssim \max(T_1,T_2)$. These results agree with the predictions from the analytical expressions for the DTLS given by Eq. (61) and hold, as will be shown, for different control- and readout-circuit parameters. It is also shown that when M_x is less than 0.6 pH $T_2 > T_1$, when M_x is larger than 0.6 pH $T_1 > T_2$, and when M_x is equal to 0.6 pH $T_1 \simeq T_2$. Hence the relaxation is the dominating source of decoherence for smaller M_x while the dephasing is the main source of decoherence for larger M_x. In addition, when $M_x < 0.1$ pH the characteristic times do not change with M_x and when $M_x \geq 0.1$ pH the characteristic times decrease with M_x monotonically. These results can be analyzed by using the analytical expressions of characteristic times for the DTLS. For example, from Eqs. (81), (72), (C8), and (C9), for small and large M_x, the relaxation time T_1 of the qubit in free decay can be well approximated by

$$T_1^{-1} \sim a_0\left(1 + b_0 M_x^2\right), \tag{94}$$

where a_0 and b_0 are two parameters independent of M_x. Eq. (94) shows that T_1 is a constant for $M_x \ll 1/\sqrt{b_0}$ and $T_1 \propto M_x^{-2}$ for $M_x \gg 1/\sqrt{b_0}$, which are in good agreement with the numerical results shown in FIG. 10. The changes of T_2, $\widetilde{T}_1$, and $\widetilde{T}_{22}$ with M_x are very similar to that of T_1 with M_x.

In FIG. 11 the characteristic times are shown versus the mutual inductance M_m between the 2D SQUID qubit and the readout circuit. It is shown that when M_m is less than 6 pH $T_1 > T_2$ and the dephasing is the main source of decoherence, when M_m is larger than 6 pH $T_2 > T_1$ and the relaxation is the dominating source of decoherence, and when $M_m \simeq 6$ pH $T_1 \simeq T_2$. It is also shown that when $M_m < 0.5$ pH the characteristic times do not change with M_m and when

$M_m \geq 0.5$ pH the characteristic times decrease monotonically with M_m. These behaviors are very similar to those of the characteristic times versus M_x. Thus the dependence of the characteristic times on M_m can also be well approximated by an equation analogous to Eq. (94).

2. Characteristic times versus readout-circuit parameters

In FIG. 12 to FIG. 15, we plot the characteristic times versus the inductances L_{J1}, L_{J2}, L_{10}, and L_{20} of the readout circuit, respectively. It is shown that the characteristic times change dramatically with L_{J1}, L_{J2}, and L_{10} but decrease slowly with L_{20}. When L_{J1} (L_{J2} or L_{10}) is less than 550 pH (100 pH or 470 pH) the characteristic times increase with L_{J1} (L_{J2} or L_{10}). When L_{J1} (L_{J2} or L_{10}) equals to 550 pH (100 pH or 470 pH) the characteristic times reach the maxima. After L_{J1} (L_{J2} or L_{10}) is larger than 550 pH (100 pH or 470 pH) the characteristic times decrease with L_{J1} (L_{J2} or L_{10}). In contrast, the characteristic times do not change much with L_{20} for very small and very large L_{20} and decrease with L_{20} for moderately large L_{20}. In addition, for all the values of inductances shown in these figures, $T_1 > T_2$. Thus the dephasing is the dominating source of decoherence

To gain insights into mechanisms behind these behaviors, we analyze these results using the analytical expressions of characteristic times for the DTLS. From Eqs. (81), (73), and (C22), at the adjacency of $\Delta L = 0$ the relaxation time T_1 of the qubit in free decay can be approximated by

$$T_1^{-1} \sim a_1 + b_1 (\Delta L)^2 , \tag{95}$$

where, $\Delta L = (L_{20} + L_{J2}) - (L_{10} + L_{J1})$, a_1 is a parameter independent of ΔL and b_1 is a parameter slowly and smoothly varying with ΔL. Eq. (95) shows that T_1 decreases with ΔL and reaches the maximum at $\Delta L = 0$.

For the results in FIG. 12, the position of the maxima of the characteristic times is at $L_{J1} = 550$ pH. This result is in very good agreement with the prediction from Eq. (95) since when $L_{J1} = 550$ pH $\Delta L = 0$. For the results in FIG. 13 and FIG. 14, we also have $\Delta L = 0$ at the positions of the maxima of the characteristic times. As for the results in FIG. 15, ΔL is always larger than 430 pH since $\Delta L = L_{20} + 430$ pH and $L_{20} \geq 0$. Thus the characteristic times do not have maxima on L_{20}.

In FIG. 16 we exhibit the characteristic times versus the capacitance C_m of the readout circuit. When $C_m < 0.01$ pF the characteristic times do not change with C_m, when 0.01 pF $\leq C_m \leq 2$ pF the characteristic times decrease with C_m , and when $C_m > 2$ pF the characteristic times tend to constants. For the values of C_m shown in this figure, $T_2 < T_1$ and thus the dephasing is the main

source of decoherence.

In FIG. 17 and FIG. 18, we show the characteristic times versus the resistances R_m and R_{m0} of the readout circuit, respectively. FIG. 17 shows that the characteristic times increase with R_m when $R_m \lesssim 1000\ \Omega$ and do not change with R_m when $R_m > 1000\ \Omega$. When R_m is less than 21 Ω $T_2 > T_1$ and the relaxation is the main source of decoherence, when R_m is larger than 21 Ω $T_1 > T_2$ and the dephasing is the dominating source of decoherence, and when R_m equals to 21 Ω $T_1 = T_2$. FIG. 18 shows that the characteristic times increase with R_{m0} when $R_{m0} \lesssim 2000\ \Omega$ and tend to constants after $R_{m0} > 2000\ \Omega$. For the values of R_{m0} shown in the figure, $T_1 > T_2$ and the dephasing is the main source of decoherence.

3. Characteristic times versus control-circuit parameters

In FIG. 19 we plot the characteristic times versus the inductance L_x of the control circuit. It is shown that when $L_x \leq 1{\times}10^2$ pH the characteristic times are constants, when $1{\times}10^2 < L_x < 1{\times}10^4$ pH the characteristic times increase with L_x, and when $L_x \geq 1 \times 10^4$ pH the characteristic times do not change with L_x. For all the values of L_x shown in this figure $T_2 < T_1$, demonstrating that the dephasing is the main source of decoherence.

In FIG. 20 the characteristic times are plotted versus the capacitance C_x of the control circuit. It is shown that the changes of the characteristic times with C_x are very similar to those with C_m. When $C_x \leq 0.05$ pF the characteristic times do not change with C_x, when $0.05 < C_x < 2.5$ pF the characteristic times decrease with C_x, and when $C_x \geq 2.5$ pF the characteristic times tend to constants. For all the values of C_x shown in this figure $T_2 < T_1$ and thus the dephasing is the main source of decoherence.

In FIG. 21 and FIG. 22 the characteristic times are plotted versus the resistances R_x and R_{x0} of the control circuit, respectively. It is shown from FIG. 21 that when R_x is less than 20 Ω $T_2 > T_1$ and the relaxation is the main source of decoherence, when R_x is larger than 20 Ω $T_1 > T_2$ and the dephasing is the dominating source of decoherence, and when R_x equals to 20 Ω $T_1 \simeq T_2$. For $R_x < 2000\ \Omega$ the characteristic times increase with R_x and for $R_x \geq 2000\ \Omega$ the characteristic times tend to constants. The changes of the characteristic times with R_{x0} shown in FIG. 22 are very similar to those with R_x. When R_{x0} is less than 2200 Ω $T_1 > T_2$ and the dephasing is the main source of decoherence, when R_{x0} is larger than 2200 Ω $T_2 > T_1$ and the relaxation is the dominating source of decoherence, and when R_{x0} is equal to 2200 Ω $T_1 = T_2$. For $R_{x0} \leq 3 \times 10^4\ \Omega$ the characteristic times increase with R_{x0} while for $R_{x0} > 3 \times 10^4\ \Omega$ the characteristic times tend

to constants.

4. Characteristic times versus temperature

Finally, we plot the characteristic times versus the temperature T of the external circuits in FIG. 23. It is shown that in general the characteristic times decrease with T. When $T \to 0$ the characteristic times tend to constants and when $T \to \infty$ the characteristic times are inversely proportional to T which is the results of classical mechanics. These results agree with the predictions from the analytical expressions of characteristic times for the DTLS. It is also shown that at the lower temperature when $T < 10.3$ mK $T_2 > T_1$ and the relaxation is the main source of decoherence, while at the higher temperature when $T > 10.3$ mK $T_1 > T_2$ and the dephasing is the dominating source of decoherence. These results also agree with the predictions from the analytical expressions for the DTLS[57] and with those obtained by others.[21,33,46].

VII. CONCLUSION

In summary, to investigate the environment-induced decoherence in realistic gate operations of solid-state qubits, we present a general theory for the treatment of decoherence of a multilevel quantum system of many degrees of freedom interacting with a multibath reservoir and driven by ac fields. In this theory, the system is described by the reduced density operator governed by the master equation. The effect of the environment on the system is characterized by the spectral density through the dissipation superoperator. The effects of driving field and leakage due to the coupling with both the driving field and environment are included in this theory. In the Hilbert space spanned by the eigenstates of the system's Hamiltonian, the reduced density operator is represented by the density matrix and the dissipation superoperator by the dissipation matrix. The diagonal and off-diagonal matrix elements of the density matrix stand for the population and coherence of the system, respectively. The dissipation matrix can be decomposed into Lamb shift matrix and damping rate matrix. They are determined by the transition matrix elements of the system and the spectral density of the environment. The effect of the Lamb shift matrix on the system is analogous to an extra field. In the case of weak damping the Lamb shift matrix is extremely small compared to the driving field and are neglected. In the study of decoherence of a qubit, for which the long-time behavior of the qubit is significant, the damping rate matrix is replaced by a steady one. For the thermal bath, the spontaneous decay rate and stimulated

transition rate are derived from the damping rate matrix. They accord with those obtained by the others with different methods and obey the detailed balance principle.

For an DTLS, the characteristic times in free and resonantly driven decays are expressed by the analytical expressions. The decoherence of the driven qubit can be decomposed into intrinsic and field-induced ones. The intrinsic decoherence time equals to the decoherence time of the qubit in free decay and the field-induced decoherence time equals to the relaxation time of the driven qubit. In the case of weak driving fields, the relaxation and thus the field-induced decoherence times of the driven qubit are independent of the field strengths and they are always in between the relaxation and decoherence times of the qubit in free decay.

For demonstration, we have applied the dissipative theory to simulate the dissipation process of the 2D SQUID qubit coupled to the external circuits in free decay. The energy levels, transition matrix elements, and relaxation time are in very good agreement with the experimental results. We have also applied the dissipative theory to investigate the effect of driving field and leakage on the decoherence of the 2D SQUID qubit coupled to the external circuits and resonantly driven by the microwave field. In the case of weak driving fields, the relaxation and decoherence times of the driven qubit are identical. They are independent of the driving field strength and in between the relaxation and decoherence times of the qubit in free decay. These results agree with the analytical results obtained from the analytical expressions of characteristic times for the DTLS. In the case of a little bit stronger driving fields, the relaxation time is sensitive to the strong field effect while the decoherence time is sensitive to the leakage. In addition, for the qubit in free decay, the relaxation is the main source of decoherence at the low temperature while the dephasing is the dominating source of decoherence at the high temperature.

To optimize the external circuits for long decoherence time, we have investigated the characteristic times of the 2D SQUID qubit change with the parameters and temperature of the control and readout circuits. We found that the characteristic times decrease with the mutual inductances and capacitances, increase with the resistances, and change dramatically with the inductances, in particular, the inductances of the readout circuit. To gain longer decoherence time, the coupling of the 2D SQUID qubit and the external circuits should be weak, the capacitances of the external circuits should be smaller, the resistances should be larger, the inductance of the control circuit should be properly larger, and in particular, to reduce the damping due to the readout circuit the total inductance of the left branch of the readout circuit should balance with that of the right branch.

Acknowledgments

We acknowledge valuable discussions with Mr. Wei Qiu and Dr. Shaoxiong Li about experimental setup. This work is supported in part by the NSF (DMR-0325551) and by AFOSR, NSA, and ARDA through DURINT grant (F49620-01-1-0439).

APPENDIX A: MASTER EQUATION OF AN OPEN QUANTUM SYSTEM

To derive the master equation for the reduced density operator of an open quantum system, we work in interaction picture. In this picture the density operator of the global system $\widetilde{\eta}(t)$ and the reduced density operator of the quantum system $\widetilde{\rho}(t)$ are defined by

$$\widetilde{\eta}(t) = \exp\left[i\left(\mathcal{L}_S + \mathcal{L}_R\right)t\right]\eta(t), \tag{A1}$$

and

$$\widetilde{\rho}(t) = \exp\left[i\mathcal{L}_S t\right]\rho(t), \tag{A2}$$

where, $\eta(t)$ and $\rho(t)$ are the density operator of the global system and the reduced density operator of the quantum system in the Schrödinger picture, respectively. The relation between $\widetilde{\rho}(t)$ and $\widetilde{\eta}(t)$ is also given by Eq. (4). Applying Eq. (A1) to Eq. (2) we obtain the *Liouville-von Neumann* for $\widetilde{\eta}(t)$ in the interaction picture

$$\frac{d\widetilde{\eta}(t)}{dt} = -i\left[\widetilde{\mathcal{L}}_F(t) + \widetilde{\mathcal{L}}_I(t)\right]\widetilde{\eta}(t), \tag{A3}$$

where, $\widetilde{\mathcal{L}}_F(t)$ and $\widetilde{\mathcal{L}}_I(t)$ are the presentations of $\mathcal{L}_F$ and $\mathcal{L}_I$ in the interaction picture. They are defined by

$$\widetilde{\mathcal{L}}_F(t) = \exp\left(i\mathcal{L}_S t\right)\mathcal{L}_F \exp\left(-i\mathcal{L}_S t\right), \tag{A4}$$

and

$$\widetilde{\mathcal{L}}_I(t) = \exp\left[i\left(\mathcal{L}_S + \mathcal{L}_R\right)t\right]\mathcal{L}_I \exp\left[-i\left(\mathcal{L}_S + \mathcal{L}_R\right)t\right], \tag{A5}$$

respectively.

The formal solution of Eq. (A3) is

$$\widetilde{\eta}(t) = \widehat{T}\exp\left[-i\int_0^t \left(\widetilde{\mathcal{L}}_F(\tau) + \widetilde{\mathcal{L}}_I(\tau)\right)d\tau\right]\widetilde{\eta}(0), \tag{A6}$$

where, $\widehat{T}$ is the time-ordering operator and $\widetilde{\eta}(0)$ is the initial density operator of the global system which is equal to $\eta(0)$ from Eq. (A1).

Suppose the reservoir is uncorrelated with the system at $t = 0$. In this case, the initial density operator of the global system $\eta(0)$ can be written as[55]

$$\eta(0) = \rho(0)\,\sigma(R), \tag{A7}$$

where, $\rho(0)$ is the reduced density operator of the system at $t = 0$ and $\sigma(R)$ is the density operator of the reservoir. For thermal baths at temperature T, for example, $\sigma(R)$ is determined by the Boltzmann distribution[52]

$$\sigma(R) = \frac{e^{-H_R/k_BT}}{\mathrm{Tr}_R\left(e^{-H_R/k_BT}\right)}, \tag{A8}$$

where, k_B is the Boltzmann constant. We also assume that (1) both the interactions H_I and H_F are weak so that the Born perturbation approximation can be applied to the exponential function of Eq. (A6);[21] (2) the reservoir is sufficiently large and its states are unperturbed by the coupling with the system and obey Gaussian statistics so that $\sigma(R)$ is time-independent, $\mathrm{Tr}_R[\sigma(R)] = 1$, and $\mathrm{Tr}_R[H_I(t)\sigma(R)] = 0$; and (3) the characteristic time of correlation is much less than the relaxation time of system so that the change of $\rho(t)$ is slow and $\rho(\tau)$ can be replaced by $\rho(t)$ in the integral over the correlation time.[56] Under the these assumptions the system will perform a Markovian process.[64] Substituting Eq. (A6) into Eq. (4), calculating the trace over the reservoir by means of the cumulant expansion method[65] under the aforementioned assumptions, and using the initial condition of Eq. (A7), we finally obtain an equation for $\widetilde{\rho}(t)$ in a series of cumulant, which is given, up to the second order of cumulant, by

$$\widetilde{\rho}(t) = \widehat{T}\exp\left\{-i\int_0^t \left[\widetilde{\mathcal{L}}_F(\tau) + i\widetilde{\mathcal{D}}_I(\tau)\right]d\tau\right\}\widetilde{\rho}(0), \tag{A9}$$

where, $\widetilde{\mathcal{D}}_I(t)$ is the dissipation superoperator in the interaction picture given by

$$\widetilde{\mathcal{D}}_I(t) = -\int_0^t \mathrm{Tr}_R\left[\widetilde{\mathcal{L}}_I(t)\,\widetilde{\mathcal{L}}_I(\tau)\,\sigma(R)\right]d\tau. \tag{A10}$$

If making transformations $\widetilde{\eta}(t) \to \widetilde{\rho}(t)$ and $\widetilde{\mathcal{L}}_I(\tau) \to i\widetilde{\mathcal{D}}_I(\tau)$ in Eq. (A6) one can get Eq. (A9). Thus if making the same transformations in Eq. (A3) one obtains an equation of motion for $\widetilde{\rho}(t)$

$$\frac{d\widetilde{\rho}(t)}{dt} = -i\widetilde{\mathcal{L}}_F(t)\widetilde{\rho}(t) + \widetilde{\mathcal{D}}_I(t)\widetilde{\rho}(t), \tag{A11}$$

This equation is recognized the master equation in the interaction picture.

Applying Eq. (A2) to Eq. (A11), one obtains the master equation for $\rho(t)$ in the Schrödinger picture

$$\frac{d\rho(t)}{dt} = -i\left[\mathcal{L}_S + \mathcal{L}_F(t)\right]\rho(t) + \mathcal{D}_I(t)\rho(t), \tag{A12}$$

where, $\mathcal{D}_I(t)$ is the representation of $\widetilde{\mathcal{D}}_I(t)$ in the Schrödinger picture given by

$$\mathcal{D}_I(t) = -\int_0^t \mathrm{Tr}_R\left[\mathcal{L}_I^S(t,\tau)\,\mathcal{L}_I^S(\tau,t)\,\sigma(R)\right]d\tau, \tag{A13}$$

with

$$\mathcal{L}_I^S(t_1,t_2) = \exp\left[-i\mathcal{L}_S t_1\right]\widetilde{\mathcal{L}}_I(t_1)\exp\left[i\mathcal{L}_S t_2\right]. \tag{A14}$$

APPENDIX B: QUANTUM LANGEVIN EQUATION AND FLUCTUATION-DISSIPATION THEOREM

We consider a quantum particle of mass M moving in a potential $V(q)$ and linearly coupled to a thermal bath at temperature T. In phase space, the motion of the quantum particle is described by the quantum Langevin equation[47]

$$M\frac{d^2q(t)}{dt^2} + M\int_{t_0}^t d\tau\gamma(t-\tau)\frac{dq(\tau)}{d\tau} + \frac{dV(q)}{dq} = \xi(t), \tag{B1}$$

where, $q(t)$ is the coordinate operator of the particle, $\gamma(t)$ is the damping coefficient, and $\xi(t)$ is the fluctuation force of the thermal bath. The quantum Langevin equation provides a relation between the damping coefficient $\gamma(t)$ and the fluctuation force $\xi(t)$ of the thermal bath.

In frequency domain, the frequency-dependent damping coefficient $\gamma(\omega)$ is calculated from $\gamma(t)$ by Fourier transform

$$\begin{aligned}\gamma(\omega) &= \gamma_R(\omega) + i\gamma_I(\omega)\\ &= \int_{-\infty}^{+\infty}\gamma(t)\exp(-i\omega t)\,dt.\end{aligned} \tag{B2}$$

The spectral density of the fluctuation force $\xi(t)$ at temperature T, $J_\xi(\omega)$, can be calculated from $\gamma_R(\omega)$ in terms of the quantum fluctuation-dissipation theorem[47,48]

$$J_\xi(\omega) = M\hbar\omega\gamma_R(\omega)\left[1+\coth\left(\frac{\hbar\omega}{2k_BT}\right)\right]. \tag{B3}$$

At high temperature limit, $T \gg \hbar\omega/k_B$ and $J_\xi(\omega)$ in Eq. (B3) is simplified to the result of the quasiclassical and classical fluctuation-dissipation theorem[47]

$$\begin{aligned}J_\xi(\omega) &= M\hbar\omega\gamma_R(\omega)\coth\left(\frac{\hbar\omega}{2k_BT}\right)\\ &\simeq 2Mk_BT\gamma_R(\omega).\end{aligned} \tag{B4}$$

It is shown that for a classical particle $J_\xi(\omega)$ is proportional to the temperature. In contrast, at low temperature limit, $T \ll \hbar\omega/k_B$ and $J_\xi(\omega)$ in Eq. (B3) is simplified to

$$J_\xi(\omega) = M\hbar\omega\gamma_R(\omega), \tag{B5}$$

which is independent of the temperature.

The autocorrelation function of the fluctuation force $\xi(t)$, $\mathcal{J}_\xi(t) = \langle\xi(t)\xi(0)\rangle$, is calculated from $J_\xi(\omega)$ by using Eq. (12). If $\gamma_R(\omega)$ is an even function of ω, the autocorrelation function of a quantum particle is given by[47]

$$\begin{aligned}\mathcal{J}_\xi(t) &= \frac{\hbar M}{\pi}\int_0^{+\infty}\omega\gamma_R(\omega)\left[i\sin(\omega t)\right. \\ &\quad \left.+\coth\left(\frac{\hbar\omega}{2k_BT}\right)\cos(\omega t)\right]d\omega.\end{aligned} \tag{B6}$$

And the autocorrelation function of a quasiclassical particle is given by

$$\begin{aligned}\mathcal{J}_\xi(t) &= \frac{\hbar M}{\pi}\int_0^{+\infty}\omega\gamma_R(\omega)\coth\left(\frac{\hbar\omega}{2k_BT}\right) \\ &\quad \times\cos(\omega t)\,d\omega.\end{aligned} \tag{B7}$$

From Eq. (B7) the autocorrelation function of the quasiclassical particle is real and reversible, i.e., $\langle\xi(t)\xi(0)\rangle = \langle\xi(-t)\xi(0)\rangle$. However, from Eq. (B6) the autocorrelation function of the quantum particle is complex and irreversible.

APPENDIX C: SPECTRAL DENSITY OF THE CONTROL AND READOUT CIRCUITS

For the 2D SQUID flux qubit shown in FIG. 1, the thermal bath consists of the control and readout circuits. They produce thermal noises for the 2D SQUID qubit.

1. Spectral density of the control circuit

As shown in FIG. 24, the control circuit is coupled to the rf SQUID through the loop L with mutual inductance M_x. The equivalent impedance Z_1 of the parallel branches C_xR_x and R_{x0} is given by

$$Z_1 = R_x^{\rm eq}(\omega) + \frac{1}{j\omega C_x^{\rm eq}(\omega)}, \tag{C1}$$

where, $R_x^{\mathrm{eq}}(\omega)$ is the frequency-dependent equivalent resistance given by

$$R_x^{\mathrm{eq}}(\omega) = \frac{1+\omega^2 C_x^2 R_x (R_x + R_{x0})}{1+\omega^2 C_x^2 (R_x + R_{x0})^2} R_{x0}, \tag{C2}$$

and $C_x^{\mathrm{eq}}(\omega)$ is the frequency-dependent equivalent capacitance given by

$$C_x^{\mathrm{eq}}(\omega) = \frac{1+\omega^2 C_x^2 (R_x + R_{x0})^2}{\omega^2 C_x R_{x0}^2}. \tag{C3}$$

When $R_{x0} \to \infty$, $R_x^{\mathrm{eq}} = R_x$ and $C_x^{\mathrm{eq}} = C_x$. When $\omega \to 0$, $R_x^{\mathrm{eq}} = R_{x0}$ and $\omega^2 C_x^{\mathrm{eq}} = 1/C_x R_{x0}^2$.

The circuit equations of the control circuit are

$$j\omega L I - j\omega M_x I_0 = U, \tag{C4}$$

$$-j\omega M_x I + (j\omega L_x + Z_1) I_0 = 0. \tag{C5}$$

From these equations, the equivalent impedance $Z_x(\omega)$ of the control circuit is given by

$$Z_x(\omega) = \frac{U}{I} = j\omega L + \frac{\omega^2 M_x^2}{j\omega L_x + Z_1}. \tag{C6}$$

From this equation, the frequency-dependent equivalent admittance $Y_x(\omega) = 1/Z_x(\omega)$ is obtained and its real part $Y_{xR}(\omega)$ is given by

$$Y_{xR}(\omega) = \frac{F_x(\omega)}{\omega^2 + G_x(\omega)}, \tag{C7}$$

where,

$$F_x(\omega) = \frac{M_x^2 R_x^{\mathrm{eq}}}{\upsilon_x^2}, \tag{C8}$$

$$G_x(\omega) = \frac{2L}{\upsilon_x C_x^{\mathrm{eq}}} + \frac{L^2}{\upsilon_x^2}\left(R_x^{\mathrm{eq}2} + \frac{1}{\omega^2 C_x^{\mathrm{eq}2}}\right), \tag{C9}$$

and

$$\upsilon_x = M_x^2 - L L_x. \tag{C10}$$

When $R_{x0} \to \infty$

$$F_x(\omega) = \frac{M_x^2 R_x}{\upsilon_x^2}, \tag{C11}$$

and

$$G_x(\omega) = \frac{2L}{\upsilon_x C_x} + \frac{L^2}{\upsilon_x^2}\left(R_x^2 + \frac{1}{\omega^2 C_x^2}\right). \tag{C12}$$

When $\omega \to 0$

$$F_x(\omega) = \frac{M_x^2 R_{x0}}{\upsilon_x^2}, \tag{C13}$$

and

$$G_x(\omega) = \frac{L^2 R_{x0}^2}{\upsilon_x^2}. \tag{C14}$$

2. Spectral density of the readout circuit

As shown in FIG. 25, the readout circuit is coupled to the rf SQUID through the loop L with mutual inductance M_m. The equivalent impedance Z_2 of the parallel branches $C_m R_m$ and R_{m0} is given by

$$Z_2 = R_m^{\mathrm{eq}}(\omega) + \frac{1}{j\omega C_m^{\mathrm{eq}}(\omega)}, \tag{C15}$$

where, $R_m^{\mathrm{eq}}(\omega)$ is the frequency-dependent equivalent resistance given by

$$R_m^{\mathrm{eq}}(\omega) = \frac{1+\omega^2 C_m^2 R_m (R_m + R_{m0})}{1+\omega^2 C_m^2 (R_m + R_{m0})^2} R_{m0}, \tag{C16}$$

and $C_m^{\mathrm{eq}}(\omega)$ is the frequency-dependent equivalent capacitance given by

$$C_m^{\mathrm{eq}}(\omega) = \frac{1+\omega^2 C_m^2 (R_m + R_{m0})^2}{\omega^2 C_m R_{m0}^2}, \tag{C17}$$

When $R_{m0} \to \infty$, $R_m^{\mathrm{eq}} = R_m$ and $C_m^{\mathrm{eq}} = C_m$. When $\omega \to 0$, $R_m^{\mathrm{eq}} = R_{m0}$ and $\omega^2 C_m^{\mathrm{eq}} = 1/C_m R_{m0}^2$.

The circuit equations of the readout circuit are given by

$$j\omega L I + j\omega \frac{M_m}{2} I_1 - j\omega \frac{M_m}{2} I_2 = U, \tag{C18}$$

$$j\omega L_1 I_1 + j\omega \frac{M_m}{2} I = j\omega L_2 I_2 - j\omega \frac{M_m}{2} I, \tag{C19}$$

and

$$j\omega L_1 I_1 + j\omega \frac{M_m}{2} I = -(I_1 + I_2) Z_2, \tag{C20}$$

where, $L_1 = L_{10} + L_{J1}$ and $L_2 = L_{20} + L_{J2}$. From these equations the equivalent admittance of the readout circuit $Y_m(\omega) = I/U$ can be obtained. Its real part is given by

$$Y_{mR}(\omega) = \frac{1}{F_m(\omega)\left[1 + G_m(\omega)\,\omega^2\right]}, \tag{C21}$$

where, $F_m(\omega)$ and $G_m(\omega)$ are given by

$$F_m(\omega) = R_m^{\mathrm{eq}} \left(\frac{L}{M_m}\right)^2 \left(\frac{2L_{dc}}{\Delta L}\right)^2 \left(1 - k_{dc}^2\right)^2, \tag{C22}$$

and

$$G_m(\omega) = \frac{1}{R_m^{\mathrm{eq}2}} \left[\frac{L_\parallel \left(1 - k_\parallel^2\right)}{1 - k_{dc}^2} - \frac{1}{\omega^2 C_m^{\mathrm{eq}}}\right]^2, \tag{C23}$$

where, $\Delta L = L_2 - L_1$, $L_{dc} = L_1 + L_2$, $L_{\|} = L_1 L_2 / L_{dc}$, $k_{dc}^2 = M_m^2 / L L_{dc}$, and $k_{\|}^2 = M_m^2 / 4 L L_{\|}$.

When $R_{m0} \to \infty$

$$F_m = R_m \left(\frac{L}{M_m} \right)^2 \left(\frac{2L_{dc}}{\Delta L} \right)^2 \left(1 - k_{dc}^2 \right)^2 , \tag{C24}$$

and

$$G_m = \frac{1}{R_m^2} \left[\frac{L_{\|} \left(1 - k_{\|}^2 \right)}{1 - k_{dc}^2} - \frac{1}{\omega^2 C_m} \right]^2 . \tag{C25}$$

When $\omega \to 0$

$$F_m = R_{m0} \left(\frac{L}{M_m} \right)^2 \left(\frac{2L_{dc}}{\Delta L} \right)^2 \left(1 - k_{dc}^2 \right)^2 , \tag{C26}$$

and

$$G_m = \frac{1}{R_{m0}^2} \left[\frac{L_{\|} \left(1 - k_{\|}^2 \right)}{1 - k_{dc}^2} - C_m R_{m0}^2 \right]^2 . \tag{C27}$$

---

[1] J. E. Mooij, T. P. Orlando, L. Levitov, L. Tian, C. H. van der Wal, and S. Lloyd, Science **285**, 1036 (1999).

[2] Y. Nakamura, Yu. A. Pashkin, and J. S. Tsai, Nature (London) **398**, 786 (1999).

[3] D. Vion, A. Aassime, A. Cottet, P. Joyez, H. Pothier, C. Urbina, D. Esteve, and M. H. Devoret, Science **296**, 886 (2002).

[4] Y. Yu, S. Han, X. Chu, S.-I. Chu, and Z. Wang, Science **296**, 889 (2002).

[5] J. M. Martinis, S. Nam, J. Aumentado, and C. Urbina, Phys. Rev. Lett. **89**, 117901 (2002).

[6] J. R. Friedman, V. Patel, W. Chen, S. K. Tolpygo, and J. E. Lukens, Nature (London) **406**, 43 (2000).

[7] C. H. van der Wal, A. C. J. ter Haar, F. K. Wilhelm, R. N. Schouten, C. J. P. M. Harmans, T. P. Orlando, S. Lloyd, and J. E. Mooij, Science **290**, 773 (2000).

[8] I. Chiorescu, Y. Nakamura, C. J. P. M. Harmans, and J. E. Mooij, Science **299**, 1869 (2003).

[9] I. Chiorescu, P. Bertet, K. Semba, Y. Nakamura, C. J. P. M. Harmans, and J. E. Mooij, Nature **431**, 159 (2004).

[10] Yu. A. Pashkin, T. Yamamoto, O. Astafiev, Y. Nakamura, D. V. Averin, and J. S. Tsai, Nature (London) **421**, 823 (2003).

[11] T. Yamamoto, Yu. A. Pashkin, O. Astafiev, Y. Nakamura, and J. S. Tsai, Nature (London) **425**, 941 (2003).

[12] A. J. Berkley, H. Xu, R. C. Ramos, M. A. Gubrud, F. W. Strauch, P. R. Johnson, J. R. Anderson, A. J. Dragt, C. J. Lobb, and F. C. Wellstood, Science **300**, 1548 (2003).

[13] R. McDermott, R. W. Simmonds, M. Steffen, K. B. Cooper, K. Cicak, K. D. Osborn, S. Oh, D. P. Pappas, and J. M. Martinis, Science **307**, 1299 (2005).

[14] R. Fazio, G. M. Palma, and J. Siewert, Phys. Rev. Lett. **83**, 5385 (1999).

[15] Z. Zhou, S.-I. Chu, and S. Han, Phys. Rev. B **66**, 054527 (2002).

[16] Z. Zhou, S.-I. Chu, and S. Han, Phys. Rev. Lett. **95**, 120501 (2005).

[17] Y. Makhlin, G. Schon, and A. Shnirman, Rev. Mod. Phys. **73**, 357 (2001).

[18] Z. Zhou, S.-I. Chu, and S. Han, Phys. Rev. B **70**, 094513 (2004).

[19] O. Astafiev, Yu. A. Pashkin, Y. Nakamura, T. Yamamoto, and J. S. Tsai, Phys. Rev. Lett. **93**, 267007 (2004).

[20] G. Ithier, E. Collin, P. Joyez, P. J. Meeson, D. Vion, D. Esteve, F. Chiarello, A. Shnirman, Y. Makhlin, J. Schriefl, and G. Schön, Phys. Rev. B **72**, 134519 (2005).

[21] G. Burkard, R. H. Koch, and D. P. DiVincenzo, Phys. Rev. B **69**, 064503 (2004).

[22] G. Burkard, D. P. DiVincenzo, P. Bertet, I. Chiorescu, and J. E. Mooij, Phys. Rev. B **71**, 134504 (2005).

[23] M. C. Goorden, M. Thorwart, and M. Grifoni, Phys. Rev. Lett. **93**, 267005 (2004).

[24] Y. Makhlin and A. Shnirman, Phys. Rev. Lett. **92**, 178301 (2004).

[25] T. P. Orlando, L. Tian, D. S. Crankshaw, S. Lloyd, C. H. van der Wal, J. Mooij, and F. Wilhelm, Physica C **368**, 294 (2002).

[26] D. J. Van Harlingen, T. L. Robertson, B. L. T. Plourde, P. A. Reichardt, T. A. Crane, and J. Clarke, Phys. Rev. Rev. B **70**, 064517 (2004).

[27] S. Shresta, C. Anastopoulos, A. Dragulescu, and B. L. Hu, Phys. Rev. A **71**, 022109 (2005).

[28] C. Anastopoulos and B. L. Hu, Phys. Rev. A **62**, 033821 (2000).

[29] T. L. Robertson, B. L. T. Plourde, T. Hime, S. Linzen, P. A. Reichardt, F. K. Wilhelm, and J. Clarke, Phys. Rev. B **72**, 024513 (2005).

[30] Y. C. Cheng and R. J. Silbey, Phys. Rev. A **69**, 052325 (2004).

[31] M. J. Storcz and F. K. Wilhelm, Phys. Rev. A **67**, 042319 (2003).

[32] M. Governale, M. Grifoni, and G. Schn, Chem. Phys. **268**, 273 (2001).

[33] L. Tian, S. Lloyd, and T. P. Orlando, Phys. Rev. B **65**, 144516 (2002).

[34] H. Xu, A. J. Berkley, R. C. Ramos, M. A. Gubrud, P. R. Johnson, F. W. Strauch, A. J. Dragt, J. R. Anderson, C. J. Lobb, and F. C. Wellstood, Phys. Rev. B **71**, 064512 (2005).

[35] G. Falci, A. D'Arrigo, A. Mastellone, and E. Paladino, Phys. Rev. Lett. **94**, 167002 (2005).

[36] Y. Nakamura, Yu. A. Pashkin, T. Yamamoto, and J. S. Tsai, Phys. Rev. Lett. **88**, 047901 (2002).

[37] K. W. Lehnert, K. Bladh, L. F. Spietz, D. Gunnarson, D. I. Schuster, P. Delsing, and R. J. Schoelkopf, Phys. Rev. Lett. **90**, 027002 (2003).

[38] T. Duty, D. Gunnarsson, K. Bladh, and P. Delsing, Phys. Rev. B **69**, 140503(R) (2004).

[39] S.-X. Li, W. Qiu, Z. Zhou, M. Matheny, W. Chen, J. E. Lukens, and S. Han, arXiv: cond-mat/0507008 (2005).

[40] P. Bertet, I. Chiorescu, G. Burkard, K. Semba, C. J. P. M. Harmans, D. DiVincenzo, and J. E. Mooij,

arXiv:cond-mat/0412485 (unpublished).

[41] A. J. Berkley, H. Xu, M. A. Gubrud, R. C. Ramos, J. R. Anderson, C. J. Lobb, and F. C. Wellstood, Phys. Rev. B **68**, 060502(R) (2003).

[42] S. K. Dutta, H. Xu, A. J. Berkley, R. C. Ramos, M. A. Gubrud, J. R. Anderson, C. J. Lobb, and F. C. Wellstood, Phys. Rev. B **70**, 140502(R) (2004).

[43] A. Barenco, C. H. Bennett, R. Cleve, D. P. DiVincenzo, N. Margolus, P. Shor, T. Sleator, J. A. Smolin, and H. Weinfurter, Phys. Rev. A **52**, 3457 (1995).

[44] M. A. Nielsen and I. L. Chuang, *Quantum Computation and Quantum Information* (Cambridge Univ. Press, Cambridge, England, 2000).

[45] Z. Zhou, S.-I. Chu, and S. Han, Phys. Rev. B **73**, 104521 (2006).

[46] A. Leggett, S. Chakravarty, A. Dorsey, M. Fisher, A. Garg, and W. Zwerger, Rev. Mod. Phys. **59**, 1 (1987).

[47] U. Weiss, *Quantum Dissipative Systems* (World Scientific Publishing Co., Singapore, 1999), 2nd ed.

[48] M. H. Devoret, in *Quantum Fluctuations*, edited by S. Reynaud, E. Giacobino, and J. Zinn-Justin, Les Houches, France, 27 June-28 July 1995 (Elsevier Science B. V., 1997), pp. 351–386.

[49] J. R. Brinati, S. S. Mizrahi, and G. A. Prataviera, Phys. Rev. A **50**, 3304 (1994).

[50] A. Yu. Smirnov, Phys. Rev. B **67**, 155104 (2003).

[51] L. Hartmann, I. Goychuk, M. Grifoni, and P. Hänggi, Phys. Rev. E **61**, R4687 (2000).

[52] W. H. Louisell, *Quantum Statistical Properties of Radiation* (John Wiley & Sons, 1973).

[53] H.-P. Breuer and F. Petruccione, *The Theory of Open Quantum Systems* (Oxford University Press, 2002).

[54] M. Toutounji, J. Chem. Phys. **123**, 244102 (2005).

[55] P. Gaspard and M. Nagaoka, J. Chem. Phys. **111**, 5668 (1999).

[56] R. Kubo, M. Toda, and N. Hashitsume, *Statistical Physics II: Nonequilibrium Statistical Mechanics* (Springer-Verlag, Berlin, 1991), 2nd ed., p. 17, 87.

[57] Z. Zhou, S.-I. Chu, and S. Han, Phys. Rev. B (submitted).

[58] N. Kosugi, S. Matsuo, K. Konno, and N. Hatakenaka, Phys. Rev. B **72**, 172509 (2005).

[59] L. Tian et al., in *Quantum Mesoscopic Phenomena and Mesoscopic Devices in Microelectronics*, edited by I. Kulik and R. Elliatioglu (2000), NATO Science Series C: Mathematical and Physical Sciences No. 559 (Kluwer Academic, Dordrecht), p. 429.

[60] S. Han, J. Lapointe, and J. Lukens, in *Single-Electron Tunneling and Mesoscopic Devices*, edited by H. Koch and Lübbig (Springer-Verlag, Berlin, 1992), vol. 31, p. 219.

[61] A. I. Larkin and Y. N. Ovchinnikov, Sov. Phys. JETP **64**, 185 (1986).

[62] S. Han et al., Science **293**, 1457 (2001).

[63] M. R. Hermann and J. A. Fleck, Jr., Phys. Rev. A **38**, 6000 (1988).

[64] G. W. Gardiner and P. Zoller, *Quantum Noise* (Springer Verlag, Berlin, 2004), 3rd ed.

[65] A. Stuart and J. K. Ord, *Kendall's Advanced Theory of Statistics, Vol. 1, Distribution Theory* (Charles Griffin and Co. Ltd, 1987), 5th ed.

Figure Captions

FIG. 1 Sketch of the 2D SQUID qubit inductively coupled to the control and readout circuits.

FIG. 2 (Online color) Contour of the potential energy of the 2D SQUID qubit.

FIG. 3 (Online color) Energy levels of the 2D SQUID qubit versus x_e.

FIG. 4 (Online color) Transition matrix elements of the 2D SQUID qubit versus x_e.

FIG. 5 (Online color) $J_x(\omega)$, $J_m(\omega)$, and $J(\omega)$ versus ω for the external circuits of the 2D SQUID flux qubit at $T = 30$ mK.

FIG. 6 (Online color) Evolution of population inversion of the 2D SQUID qubit in free decay. The solid and dashed lines are the numerical and fitting results, respectively.

FIG. 7 (Online color) Same as FIG. 6 but for the squared modulus of coherence.

FIG. 8 (Online color) Evolution of population difference of the 2D SQUID qubit resonantly driven by the microwave field with $\phi_\mu = 1.0 \times 10^{-5}$ and $\omega_\mu = \omega_{21} = 0.127\omega_{LC}$. The solid and dashed lines are the numerical and fitting results, respectively.

FIG. 9 (Online color) Same as FIG. 8 but for the squared modulus of coherence.

FIG. 10 (Online color) Characteristic times versus the mutual inductance M_x between the 2D SQUID qubit and the control circuit. In this figure, T_1 and T_2 are the relaxation and decoherence times of the qubit in free decay, and $\widetilde{T}_1$ and $\widetilde{T}_{22}$ are the relaxation and decoherence times of the qubit in driven decay.

FIG. 11 (Online color) Same as FIG. 10 but for characteristic times versus the mutual inductance M_m between the 2D SQUID qubit and the readout circuit.

FIG. 12 (Online color) Same as FIG. 10 but for characteristic times versus the inductance L_{J1} of the first junction of the readout circuit.

FIG. 13 (Online color) Same as FIG. 10 but for characteristic times versus the inductance L_{J2} of the second junction of the readout circuit.

FIG. 14 (Online color) Same as FIG. 10 but for characteristic times versus the inductance L_{10} of the readout circuit.

FIG. 15 (Online color) Same as FIG. 10 but for characteristic times versus the inductance L_{20} of the readout circuit.

FIG. 16 (Online color) Same as FIG. 10 but for characteristic times versus the capacitance C_m of the readout circuit.

FIG. 17 (Online color) Same as FIG. 10 but for characteristic times versus the resistance R_m of the readout circuit.

FIG. 18 (Online color) Same as FIG. 10 but for characteristic times versus the resistance R_{m0} of the readout circuit.

FIG. 19 (Online color) Same as FIG. 10 but for characteristic times versus the inductance L_x of the control circuit.

FIG. 20 (Online color) Same as FIG. 10 but for characteristic times versus the capacitance C_x of the control circuit.

FIG. 21 (Online color) Same as FIG. 10 but for characteristic times versus the resistance R_x of the control circuit.

FIG. 22 (Online color) Same as FIG. 10 but for characteristic times versus the resistance R_{x0} of the control circuit.

FIG. 23 (Online color) Same as FIG. 10 but for characteristic times versus the temperature T.

FIG. 24 The control circuit of the 2D SQUID flux qubit and its equivalent admittance $Y_x(\omega)$.

FIG. 25 The readout circuit of the 2D SQUID flux qubit and its equivalent admittance $Y_m(\omega)$.

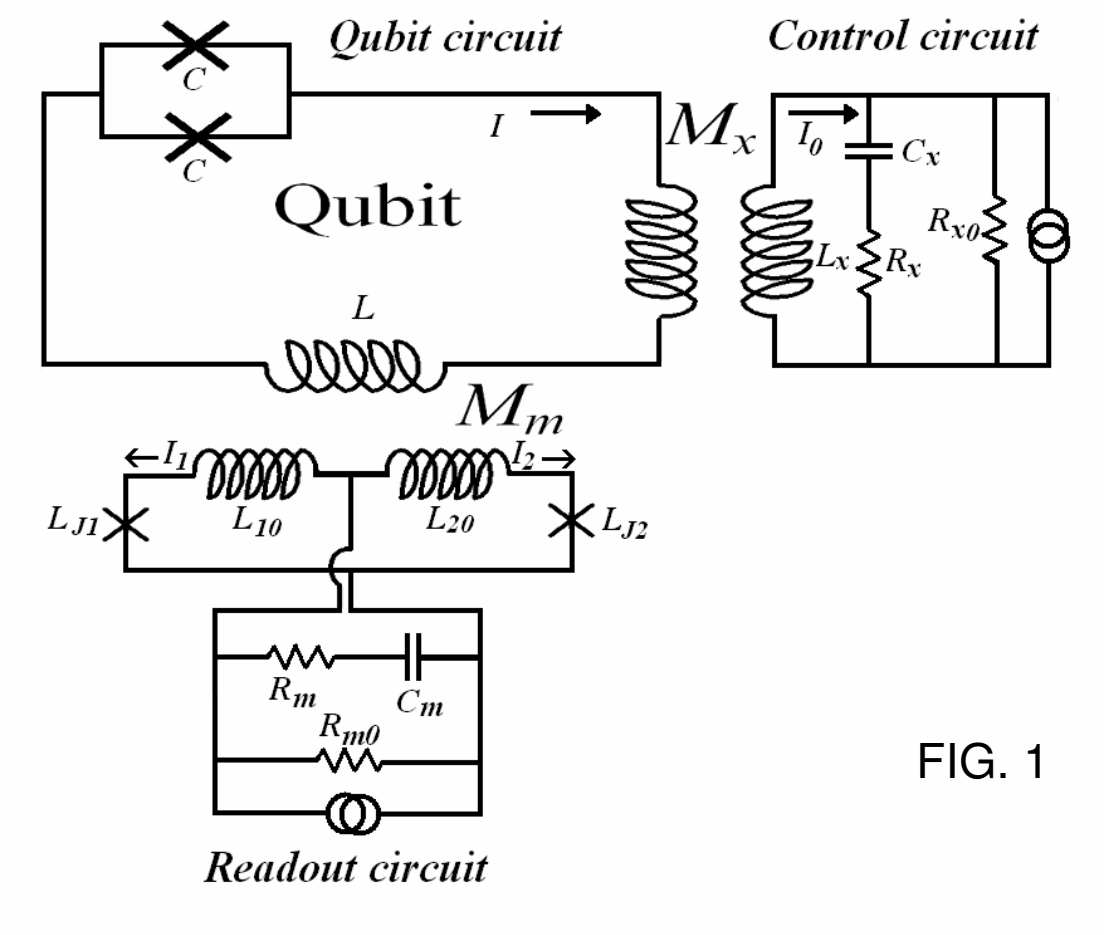
Qubit circuit
Control circuit
C
C
I
M_x
I_0
C_x
Qubit
R_{x0}
L_x
R_x
L
M_m
I_1
I_2
L_{J1}
L_{10}
L_{20}
L_{J2}
R_m
C_m
R_{m0}
Readout circuit

FIG. 1

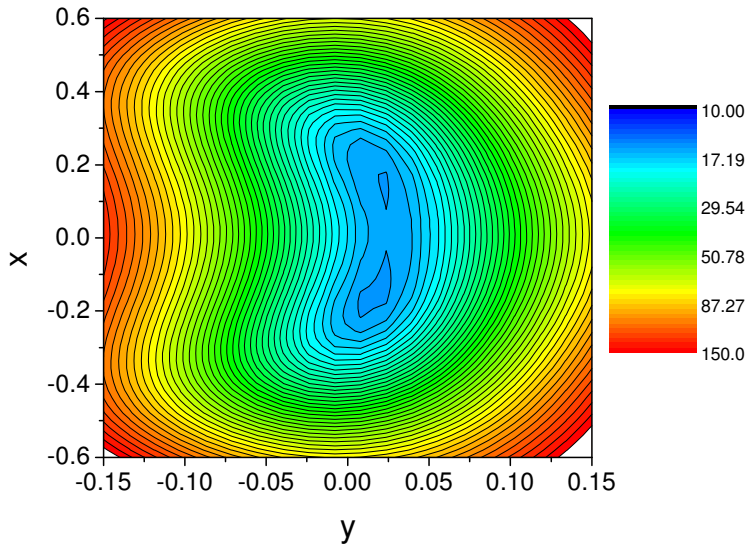
0.6
0.4
0.2
0.0
-0.2
-0.4
-0.6
x
-0.15
-0.10
-0.05
0.00
0.05
0.10
0.15
y
10.00
17.19
29.54
50.78
87.27
150.0

FIG. 2

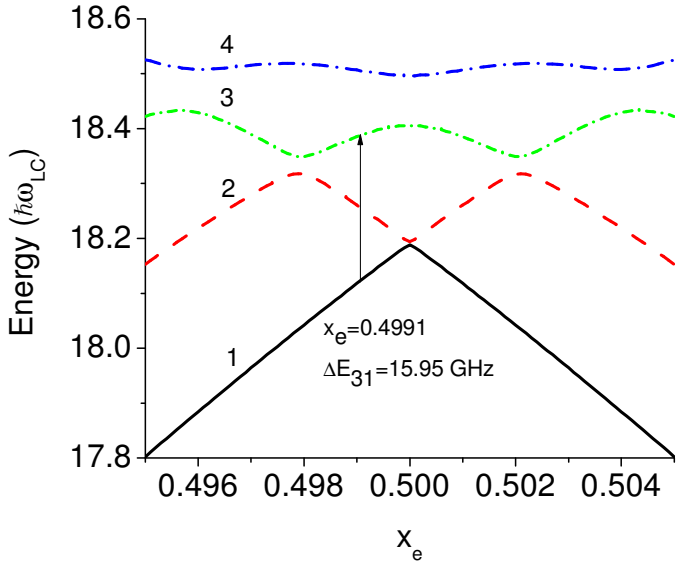
18.6
18.4
18.2
18.0
17.8
Energy ($\hbar\omega_{LC}$)
4
3
2
1
x_e=0.4991
ΔE_{31}=15.95 GHz
0.496
0.498
0.500
0.502
0.504
x_e

FIG. 3

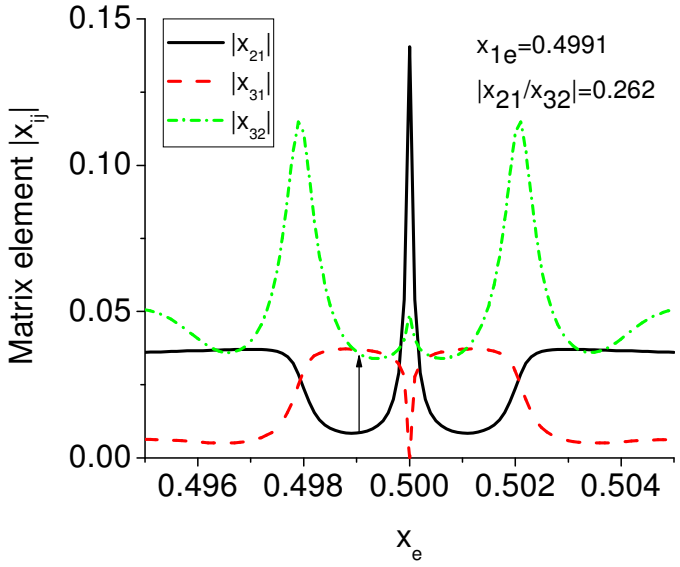
0.15
0.10
0.05
0.00
Matrix element |x_ij|
|x_21|
|x_31|
|x_32|
x_1e=0.4991
|x_21/x_32|=0.262
0.496
0.498
0.500
0.502
0.504
x_e

FIG. 4

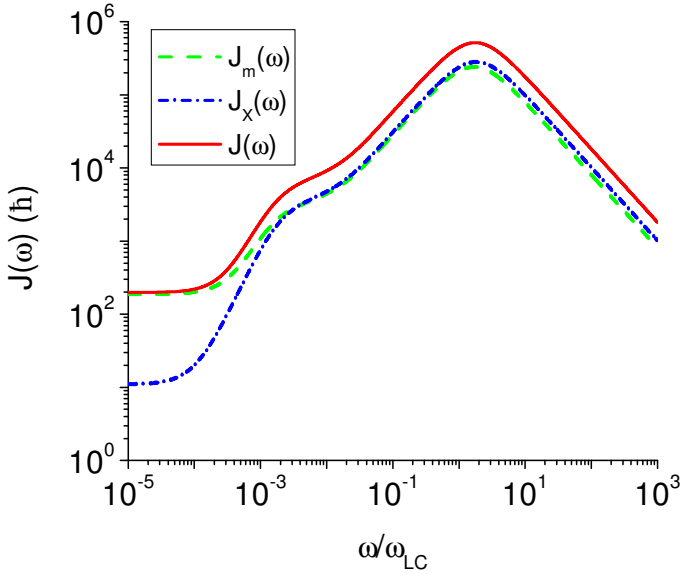
10^6
10^4
10^2
10^0
J(ω) (ħ)
$J_m(\omega)$
$J_X(\omega)$
J(ω)
10^{-5}
10^{-3}
10^{-1}
10^1
10^3
ω/ω_{LC}

FIG. 5

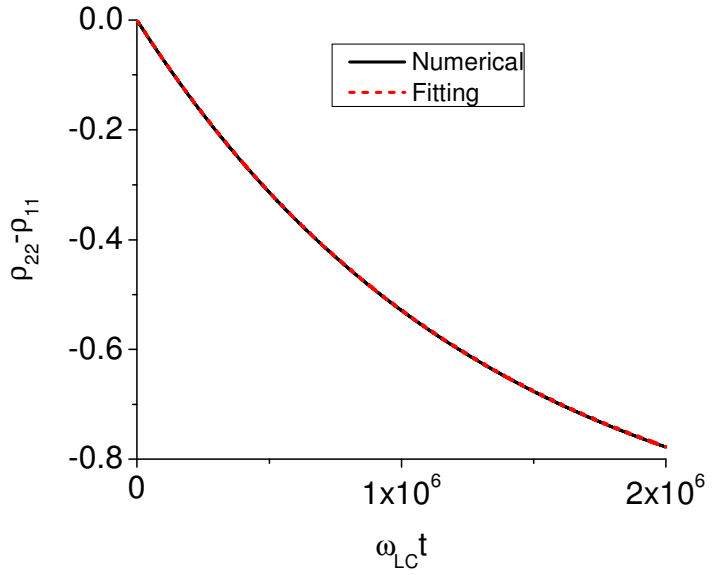
0.0
-0.2
-0.4
-0.6
-0.8
ρ_{22}-ρ_{11}
0
1x10^6
2x10^6
ω_{LC}t
Numerical
Fitting

FIG. 6

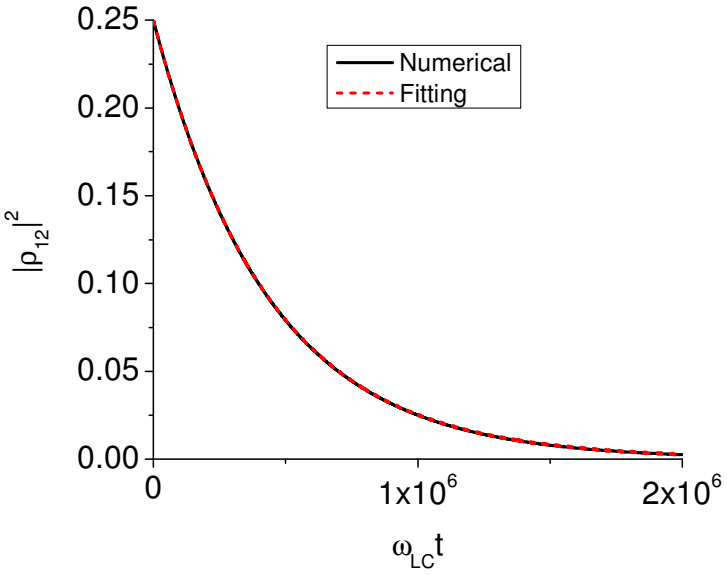
0.25
0.20
0.15
0.10
0.05
0.00
$|\rho_{12}|^2$
Numerical
Fitting
0
1x10^6
2x10^6
$\omega_{LC}t$

FIG. 7

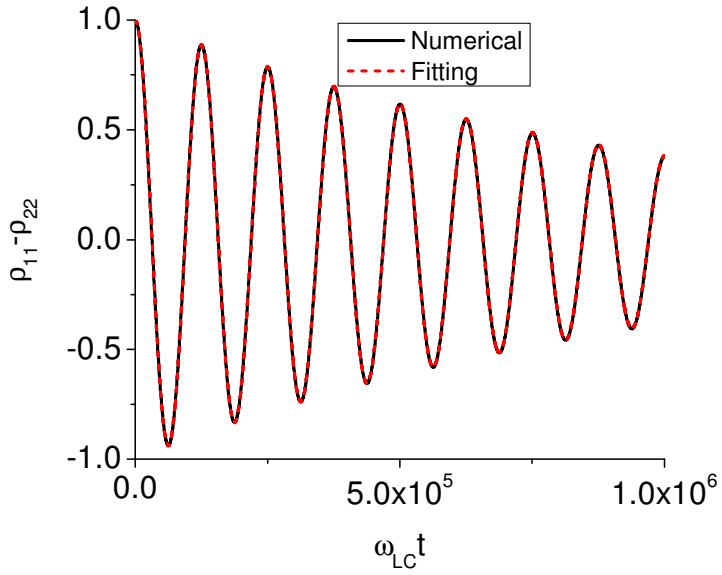
1.0
0.5
0.0
-0.5
-1.0
0.0
5.0x10^5
1.0x10^6
ρ11-ρ22
ωLCt
Numerical
Fitting

FIG. 8

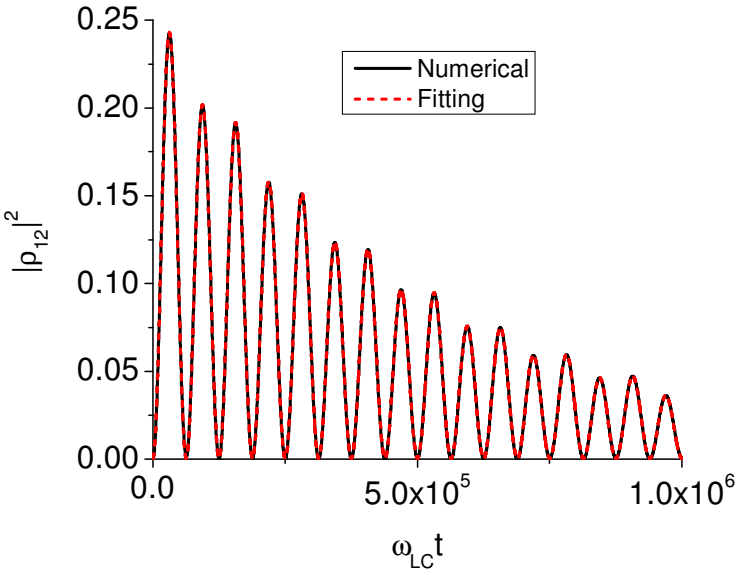
0.25
0.20
0.15
0.10
0.05
0.00
$|\rho_{12}|^2$
Numerical
Fitting
0.0
5.0x10^5
1.0x10^6
$\omega_{LC}t$

FIG. 9

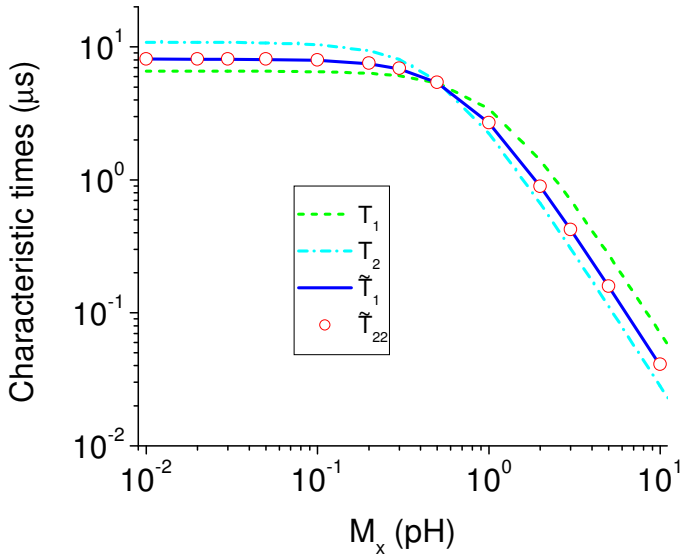
Characteristic times (μs)
10^{1}
10^{0}
10^{-1}
10^{-2}
10^{-2}
10^{-1}
10^{0}
10^{1}
M_x (pH)
T_1
T_2
$\tilde{T}_1$
$\tilde{T}_{22}$

FIG. 10

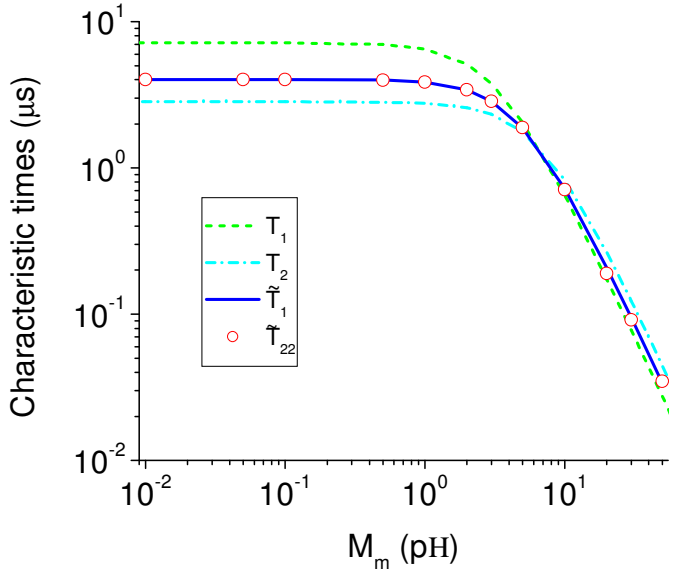
Characteristic times (μs)
10^{1}
10^{0}
10^{-1}
10^{-2}
10^{-2}
10^{-1}
10^{0}
10^{1}
M_m (pH)
T_1
T_2
$\tilde{T}_1$
$\tilde{T}_{22}$

FIG. 11

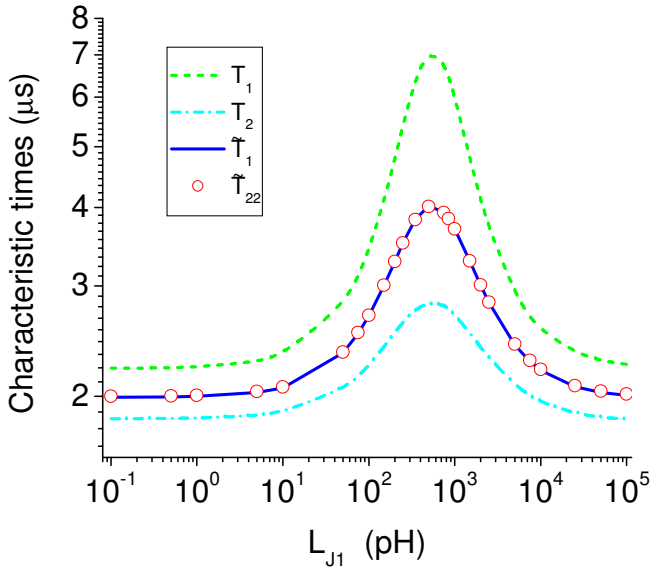
Characteristic times (μs)
8
7
6
5
4
3
2
T_1
T_2
$\tilde{T}_1$
$\tilde{T}_{22}$
10^{-1}
10^{0}
10^{1}
10^{2}
10^{3}
10^{4}
10^{5}
L_{J1} (pH)

FIG. 12

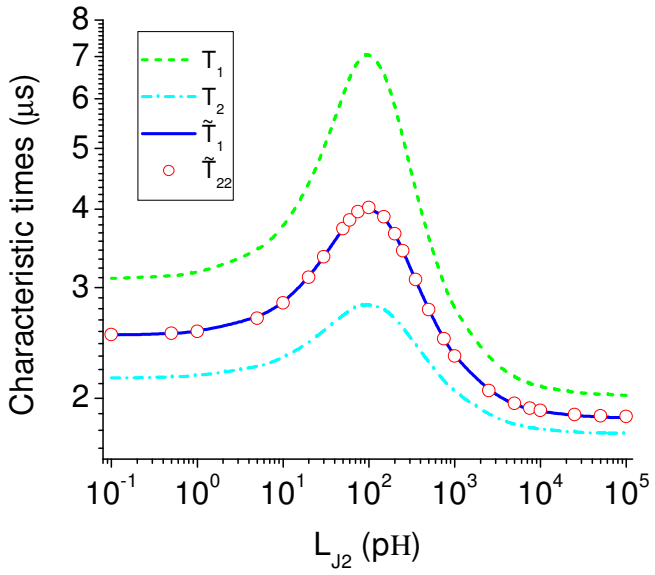
Characteristic times (μs)
8
7
6
5
4
3
2
T1
T2
T̃1
T̃22
10-1
100
101
102
103
104
105
LJ2 (pH)

FIG. 13

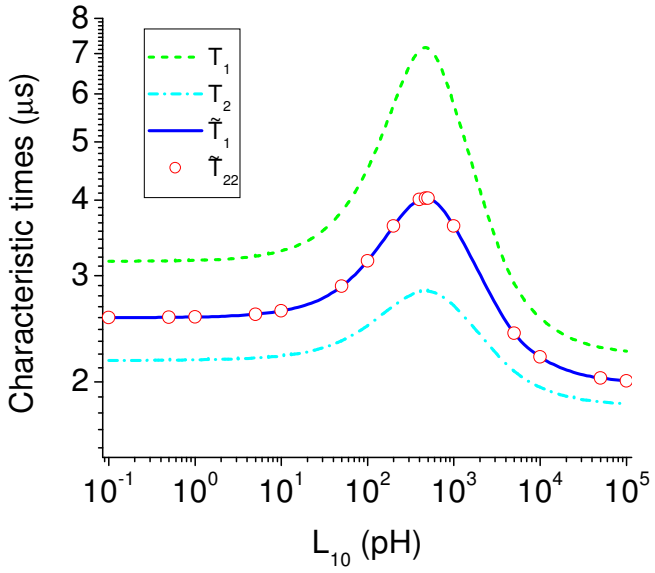
Characteristic times (μs)
8
7
6
5
4
3
2
T1
T2
T̃1
T̃22
10-1
100
101
102
103
104
105
L10 (pH)

FIG. 14

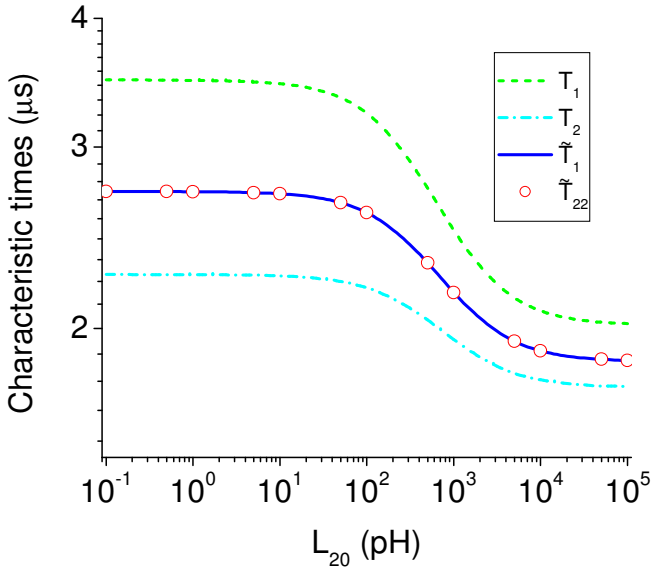
Characteristic times (μs)
4
3
2
10^{-1}
10^{0}
10^{1}
10^{2}
10^{3}
10^{4}
10^{5}
L_{20} (pH)
T_1
T_2
$\tilde{T}_1$
$\tilde{T}_{22}$

FIG. 15

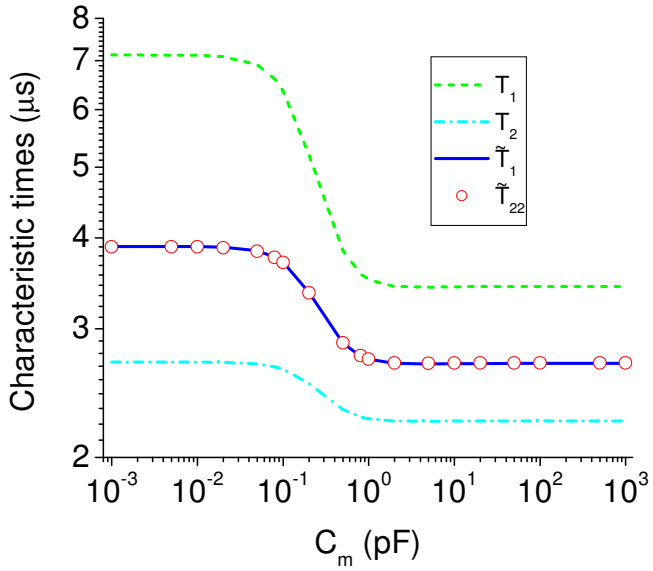
Characteristic times (μs)
8
7
6
5
4
3
2
10^{-3}
10^{-2}
10^{-1}
10^{0}
10^{1}
10^{2}
10^{3}
C_m (pF)
T_1
T_2
$\tilde{T}_1$
$\tilde{T}_{22}$

FIG. 16

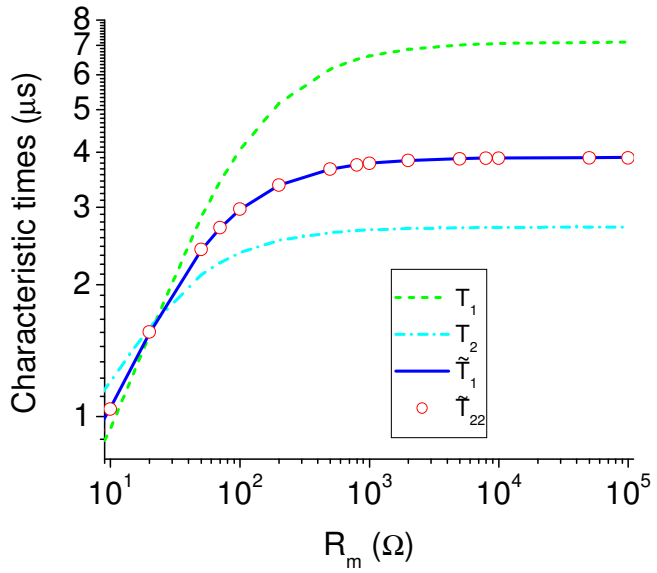
Characteristic times (μs)
8
7
6
5
4
3
2
1
10^1
10^2
10^3
10^4
10^5
R_m (Ω)
T_1
T_2
$\tilde{T}_1$
$\tilde{T}_{22}$

FIG. 17

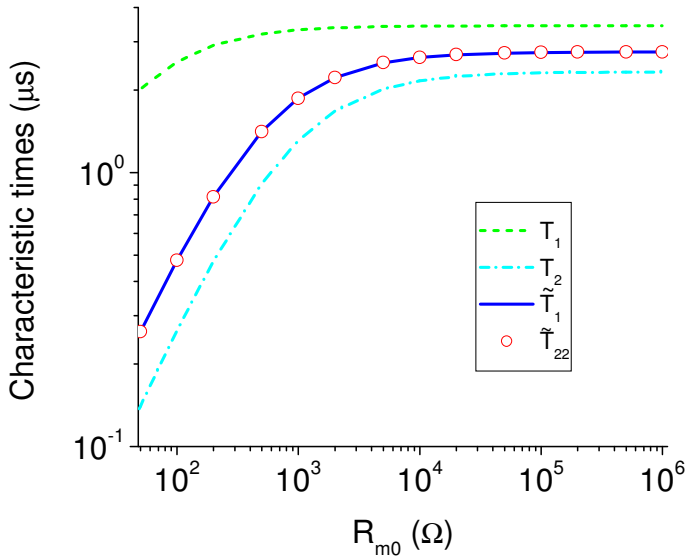
Characteristic times (μs)
10^0
10^-1
10^2
10^3
10^4
10^5
10^6
R_m0 (Ω)
T_1
T_2
T̃_1
T̃_22

FIG. 18

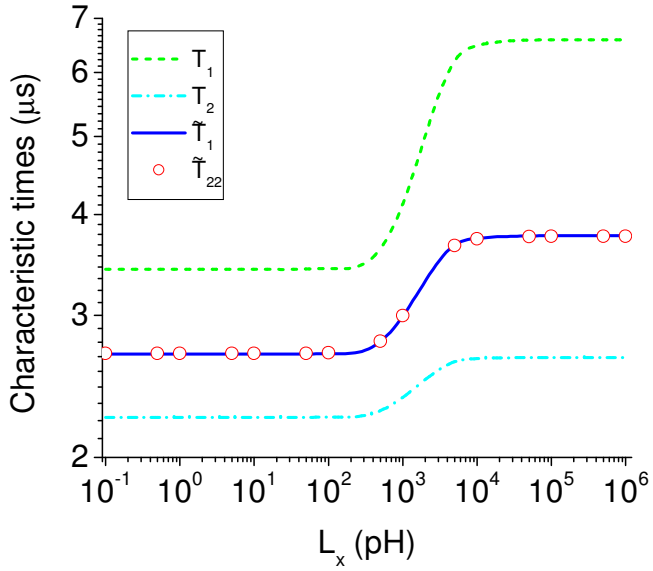
Characteristic times (μs)
7
6
5
4
3
2
T1
T2
T̃1
T̃22
10-1
100
101
102
103
104
105
106
Lx (pH)

FIG. 19

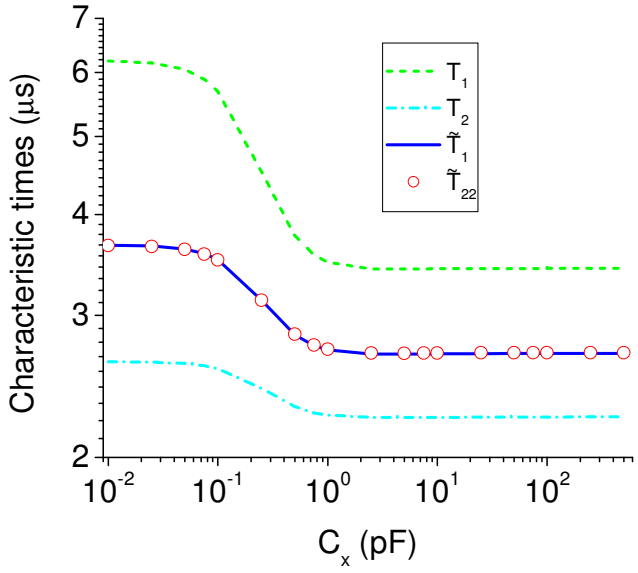
Characteristic times (μs)
7
6
5
4
3
2
10^{-2}
10^{-1}
10^{0}
10^{1}
10^{2}
C_x (pF)
T_1
T_2
$\tilde{T}_1$
$\tilde{T}_{22}$

FIG. 20

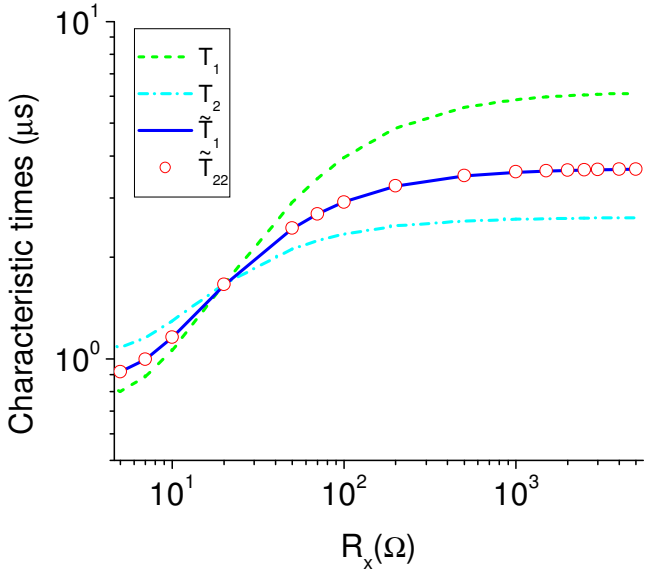
Characteristic times (μs)
10^1
10^0
T_1
T_2
$\tilde{T}_1$
$\tilde{T}_{22}$
10^1
10^2
10^3
$R_x(\Omega)$

FIG. 21

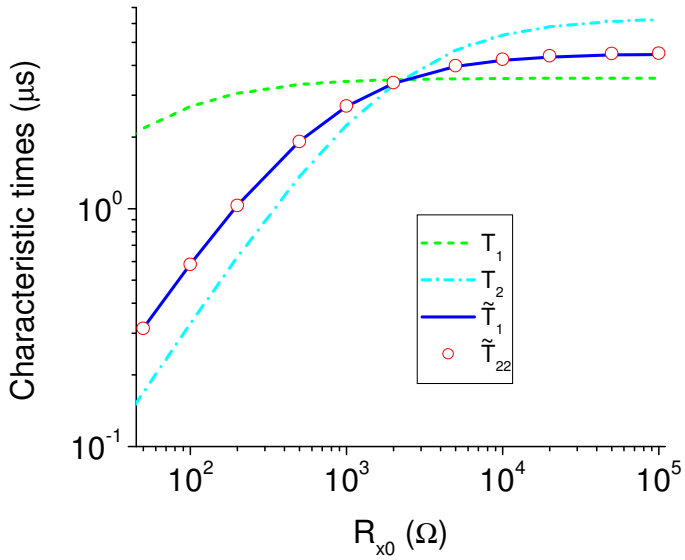
Characteristic times (μs)
10^0
10^-1
10^2
10^3
10^4
10^5
R_x0 (Ω)
T_1
T_2
T̃_1
T̃_22

FIG. 22

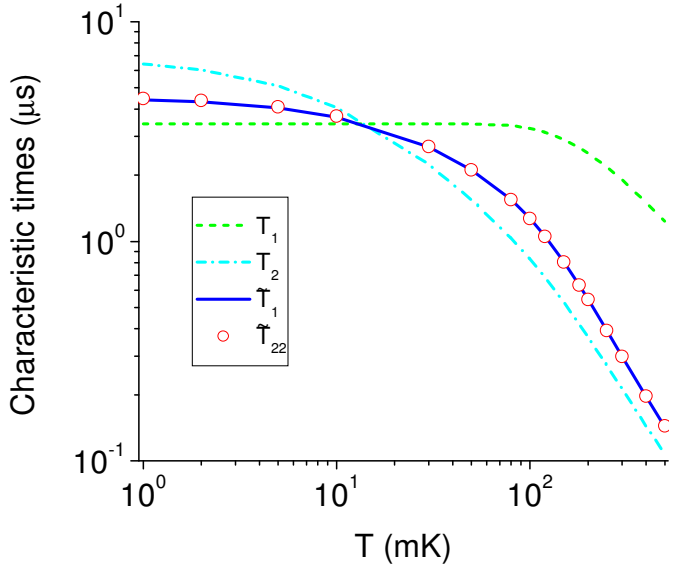
Characteristic times (μs)
T (mK)
10^1
10^0
10^{-1}
10^0
10^1
10^2
T_1
T_2
$\tilde{T}_1$
$\tilde{T}_{22}$

FIG. 23

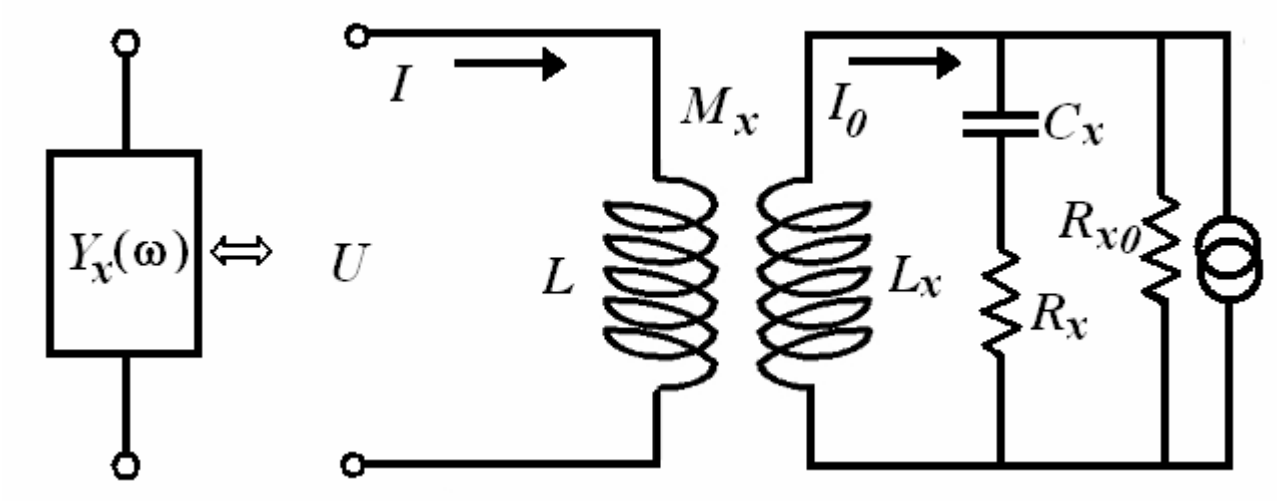

FIG. 24

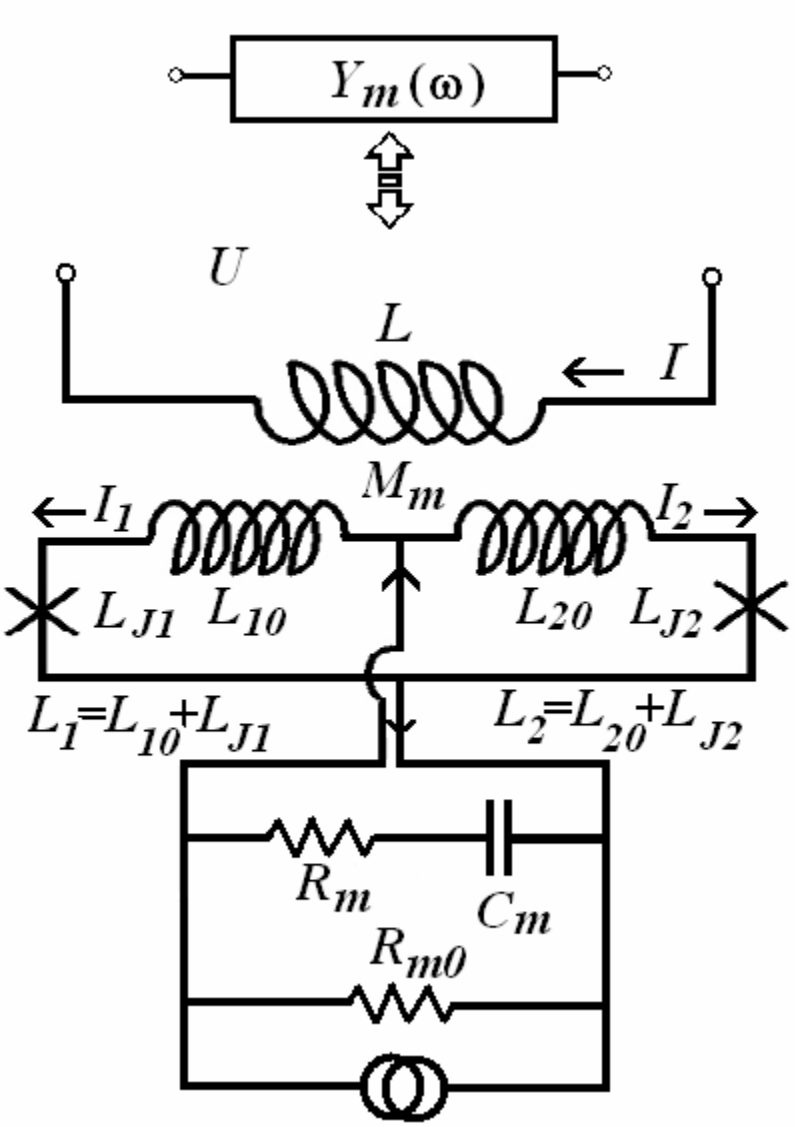
$Y_m(\omega)$
U
L
I
M_m
I_1
I_2
L_{J1}
L_{10}
L_{20}
L_{J2}
$L_1=L_{10}+L_{J1}$
$L_2=L_{20}+L_{J2}$
R_m
C_m
R_{m0}

FIG. 25